Future Astrophysical Targets for Intensity Interferometry

Neal Dalal, Marios Galanis, Charles Gammie, Samuel Gralla, Norman Murray

Dalal et al. (2024)

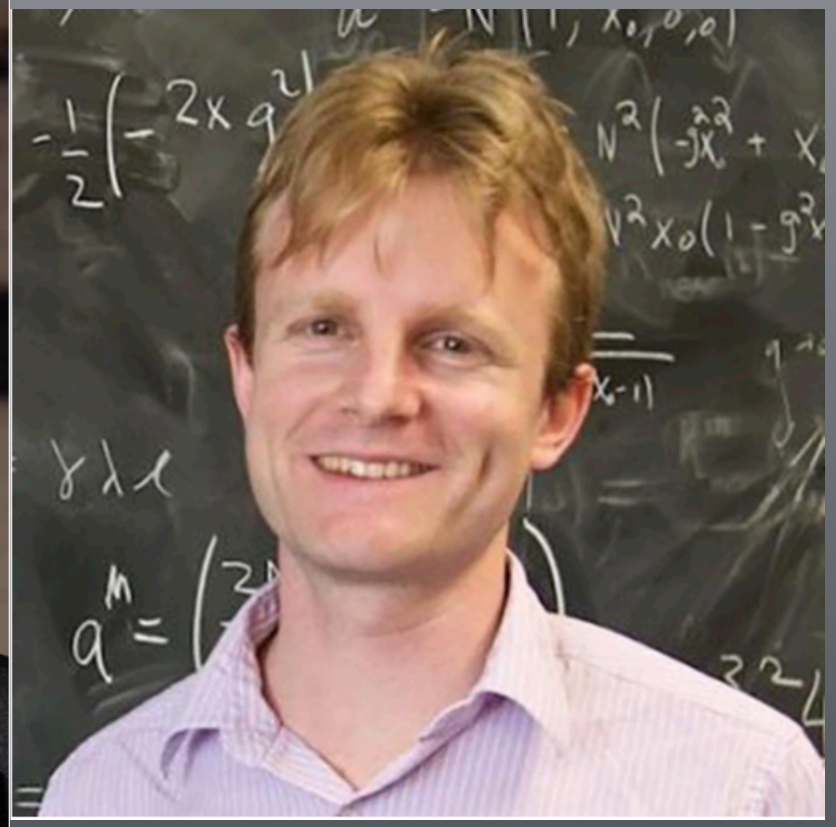

Intensity Interferometry

Hanbury Brown & Twiss

- Similar to interferometry in the radio or millimeter band (amplitude interferometry)
- Use large base lines **B** and short wavelengths λ to get high angular resolution
  - $\theta \sim \lambda/B$
  - $\lambda \sim 5000$ angstroms or 5×10^{-5} cm, $B \sim 10^4$ km, $\theta \sim 0.01\mu$ arcseconds
  - AGN disks $R_s \sim 3\text{x}10^{13}$ cm, $D \sim 100$Mpc, $\theta \sim 20\mu$ arcseconds
  - Stellar disks $R_\odot \sim 7\text{x}10^{10}$ cm, $D \sim 10$ pc, $\theta \sim 0.5$ milliarcseconds
    - Can get many resolution elements across the stellar disk

Possible Astrophysical Targets

- AGN
- Green Peas/LRDs
- Resolved Asteroseismology
- Later talks
  - H_0 (Marios—-next talk)
  - Supernovae
- Not covered:
  - Photon rings
  - Tidal Disruption Events

Possible Astrophysical Targets

- AGN
  - Disk angular size
  - Disk scale height
    - Thin versus thick
  - Map Broad Line Region
    - Determine where outflows emerge
  - Binary supermassive black holes (OJ 287)
  - Green Peas/Little Red Dots (LRDs)
- Resolved Asteroseismology
  - 2D power spectra (velocity versus l)
    - Run of Temperature
    - Rotational splitting $\Rightarrow$ Internal differential rotation

AGN Broad Line Region

Credit: Neal Dalal

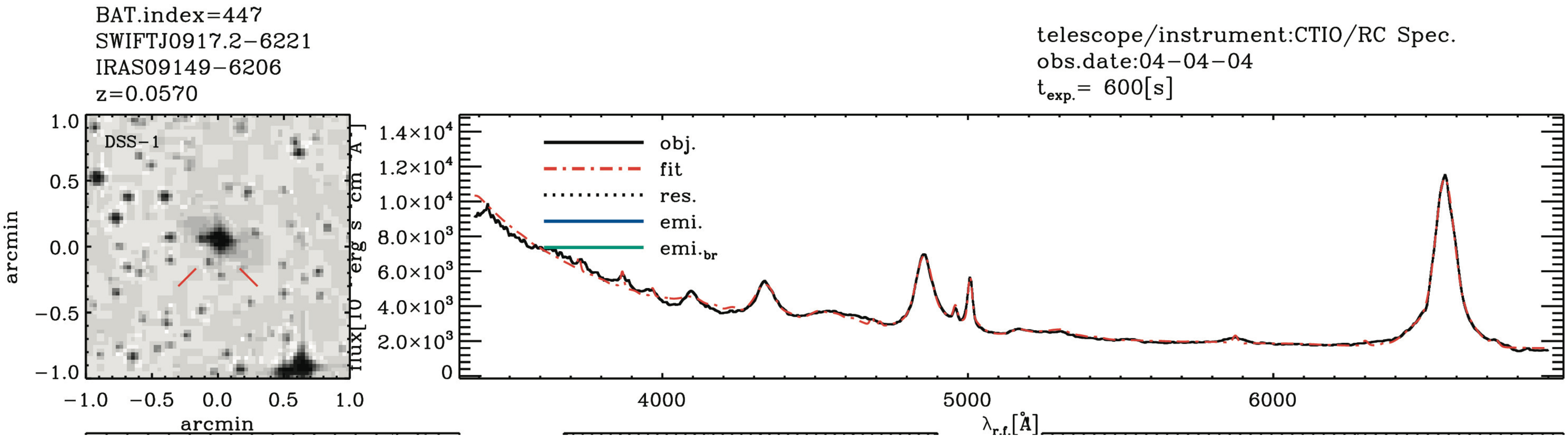

Credit: Neal Dalal

AGN variability

- AGN luminosity varies over time, for both continuum and lines.
- But line variability **lags** the continuum variability.
- Time lags can be days - months

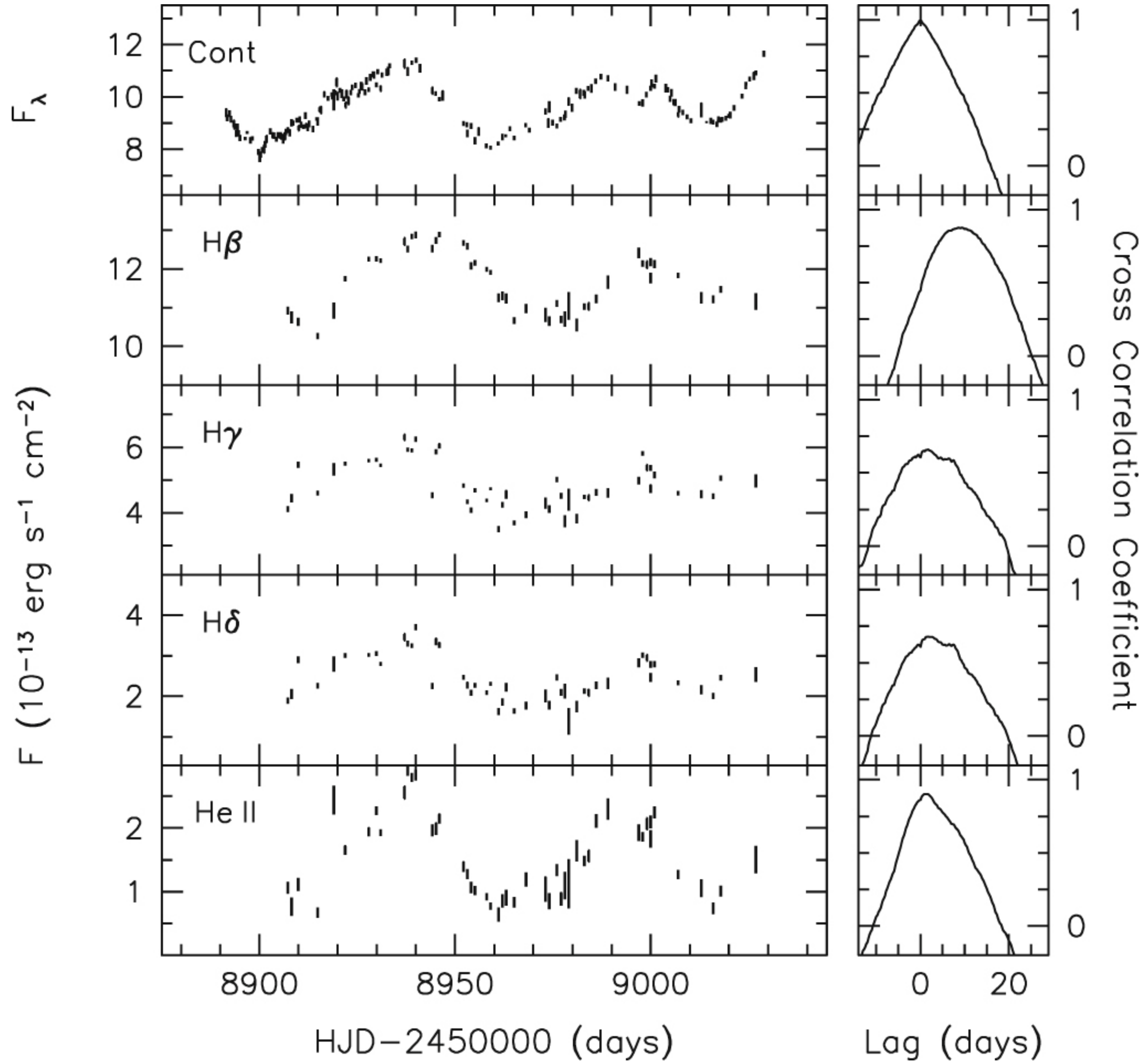

NGC 3783 V~14

Bentz et al. (2021)

Credit: Neal Dalal

IRAS 09149-6206

24hours, CTA-sized array

For AGN science, all these numbers are interesting!

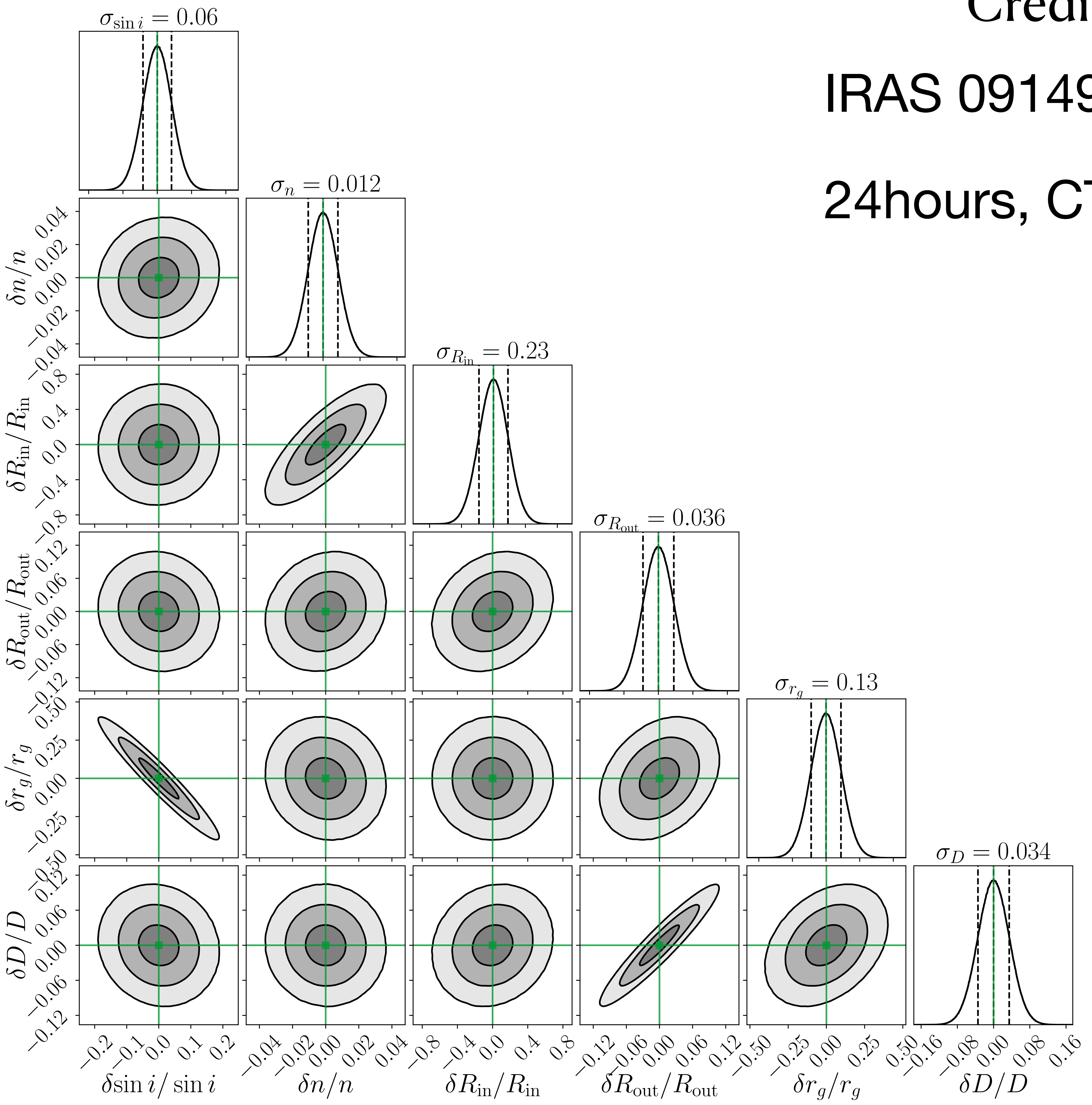

Distance is interesting for cosmology

AGN: Thin Disks?

FORGE'd in FIRE Hopkins et al

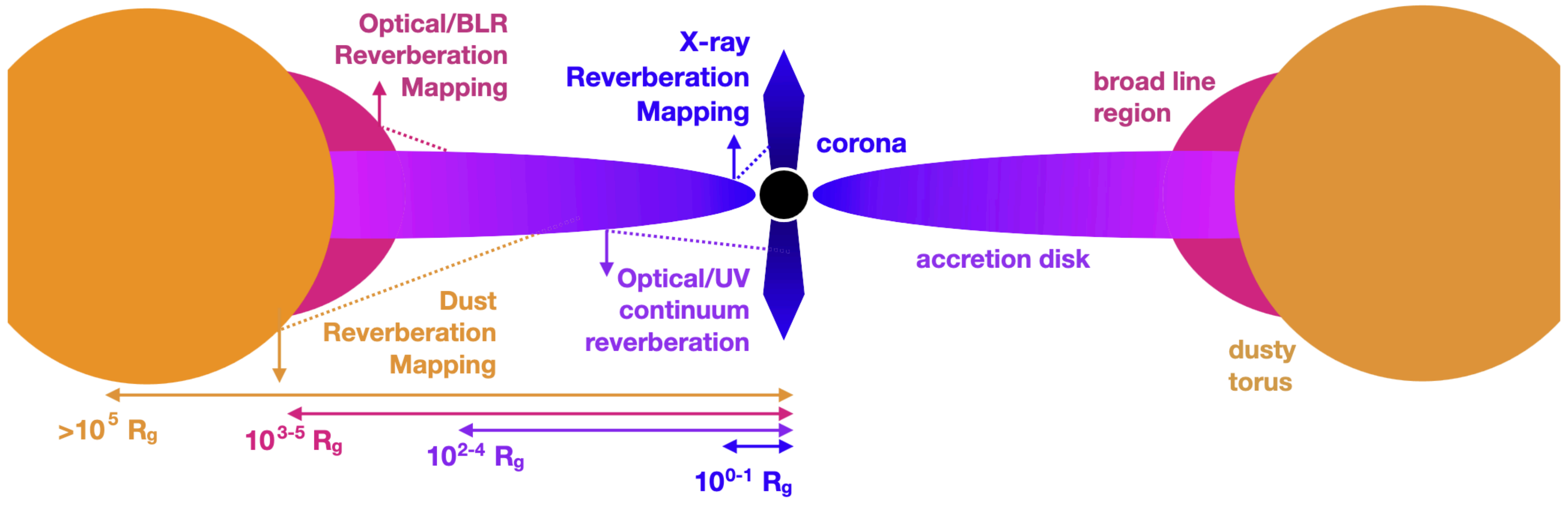

FORGE'd in FIRE II 5

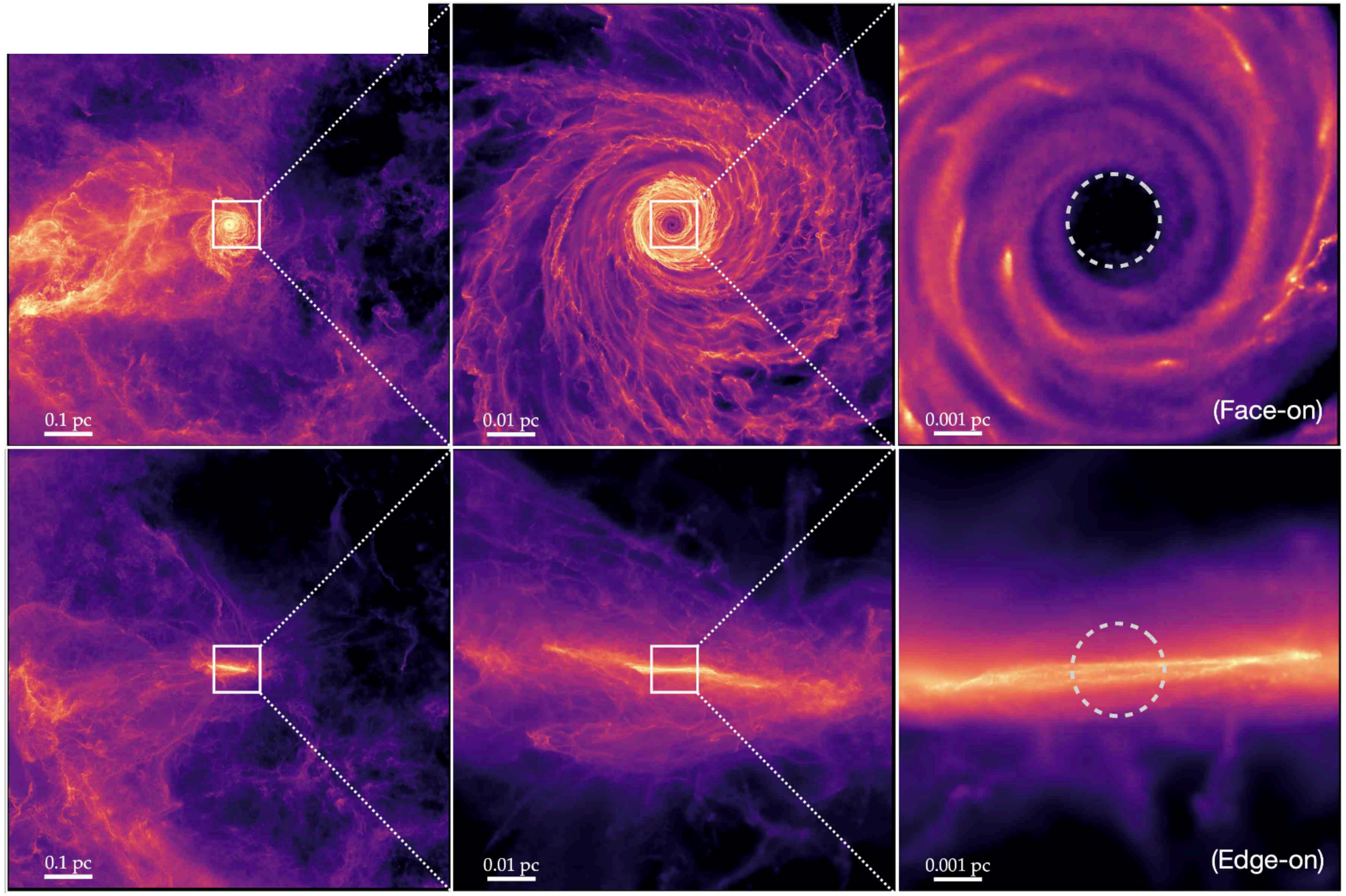

AGN: Thin Disks?

FORGE'd in FIRE Hopkins et al

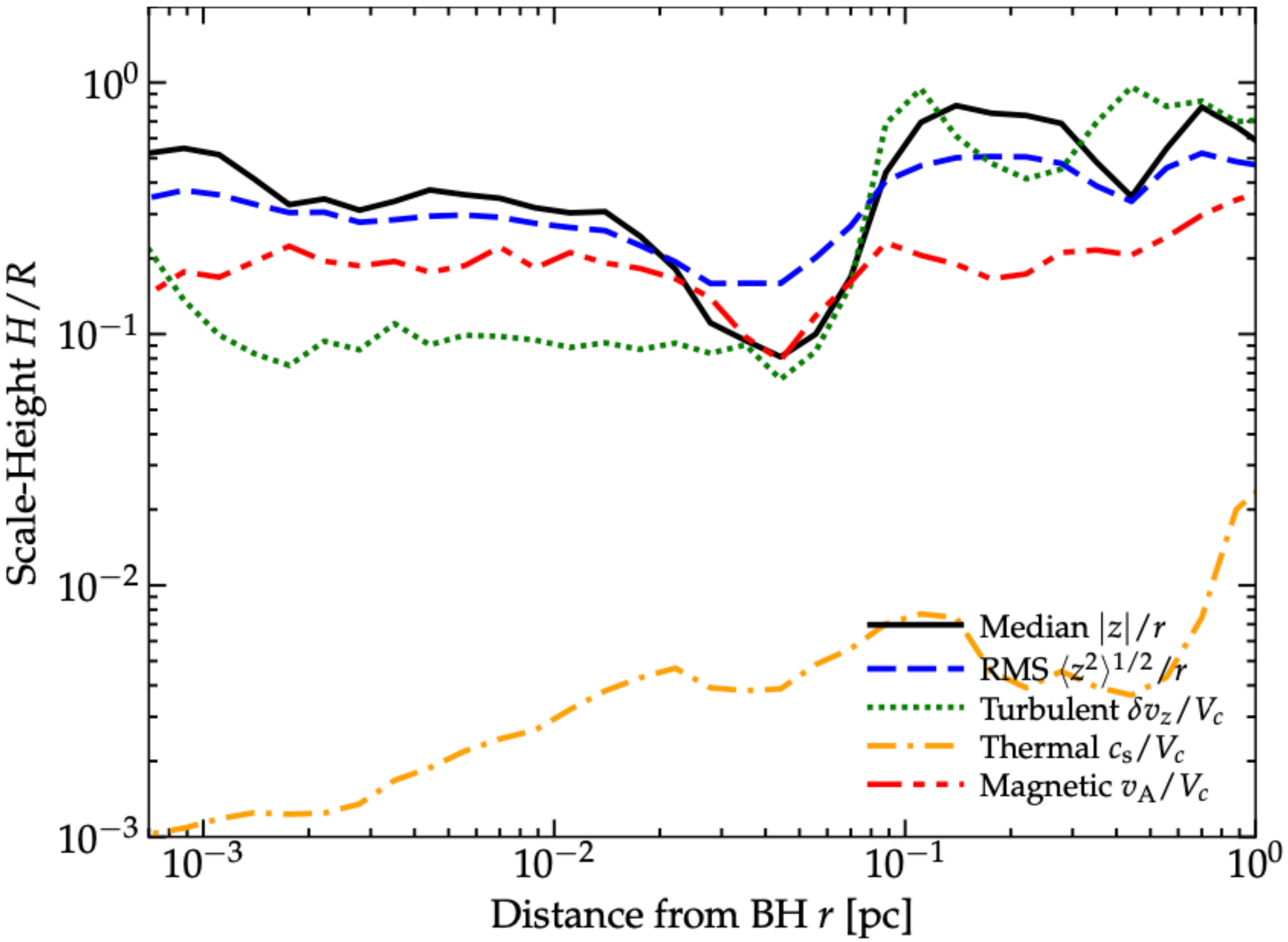

AGN: Thin Disks?

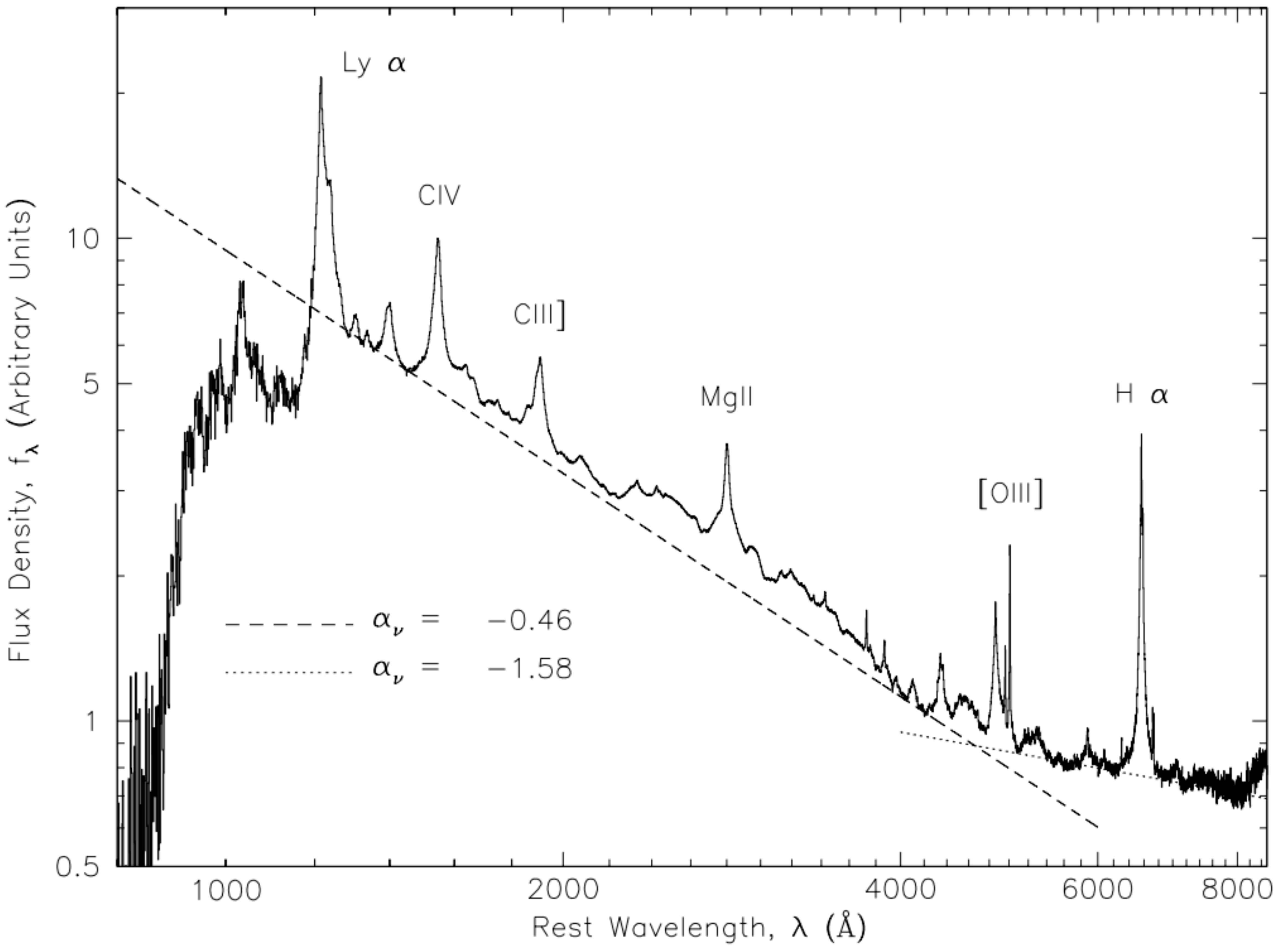

Fig. 3.—Composite quasar spectrum using median combining. Power-law fits to the estimated continuum flux are shown. The resolution of the input spectra is ≈1800, which gives a wavelength resolution of about 1 Å in the rest frame.

Feedback in galaxy formation

Stellar mass to halo mass estimates

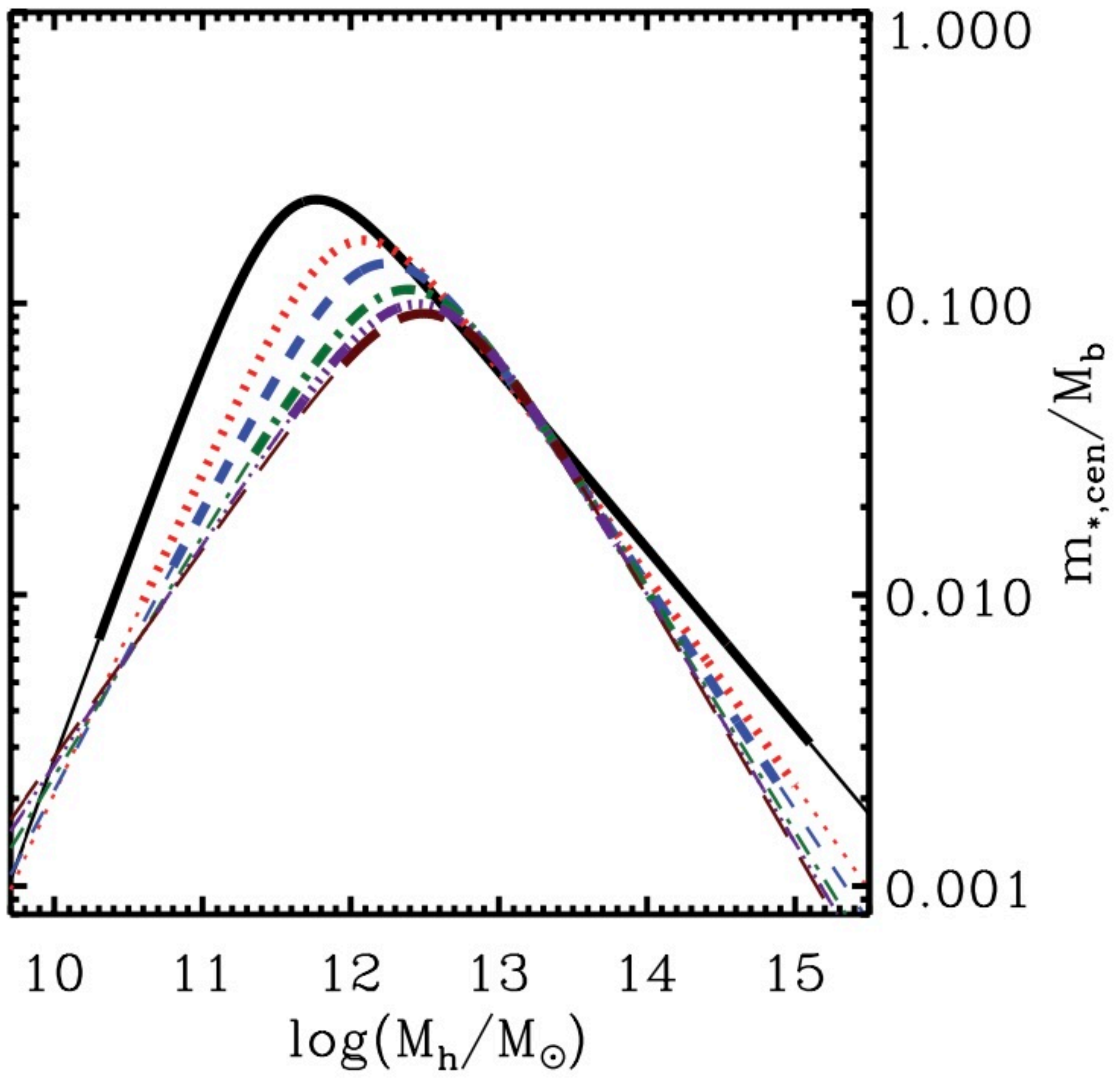

Moster et al 2013

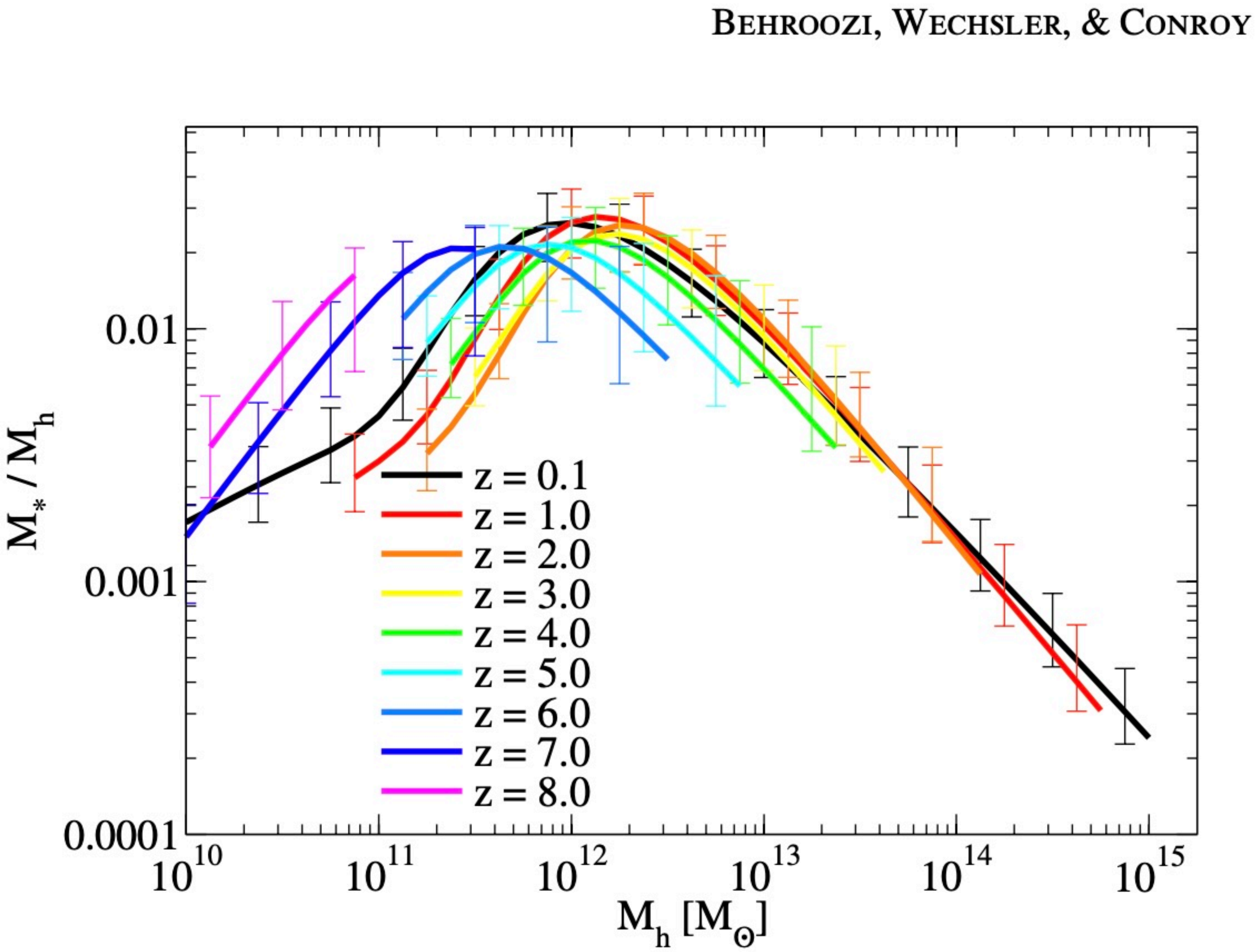

Ferrarese & Merritt 2000

BAL Outflows & Galaxy Evolution

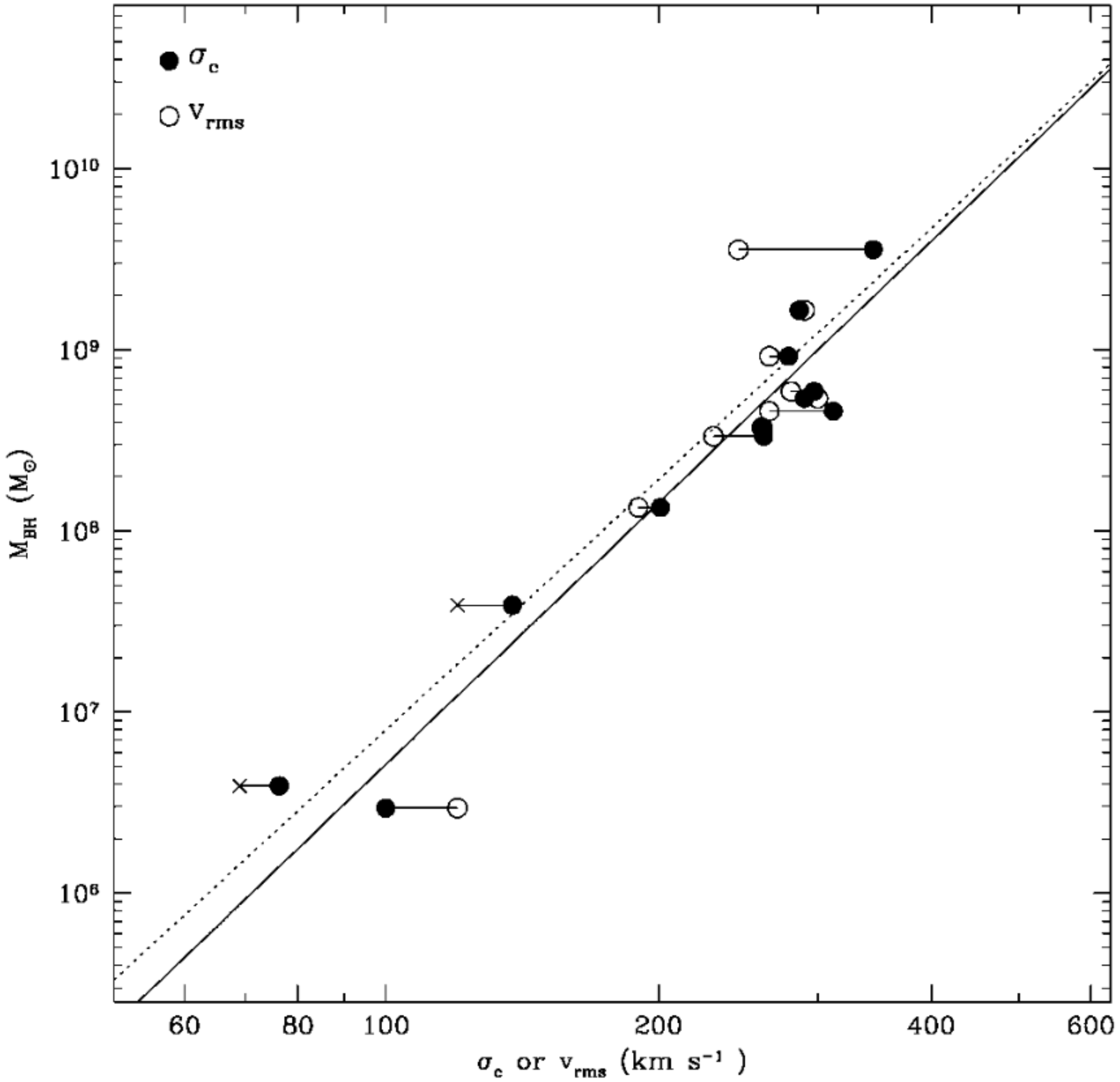

FIG. 2.—BH mass vs. the central velocity dispersion σ_c of the host elliptical galaxy or bulge (*filled circles*) or the rms velocity v_{rms} measured at one-fourth of the effective radius (*open circles*). Crosses represent lower limits in v_{rms}. The solid and dashed lines are the best linear fits using σ_c (as in Fig. 1*b*) and v_{rms}, respectively.

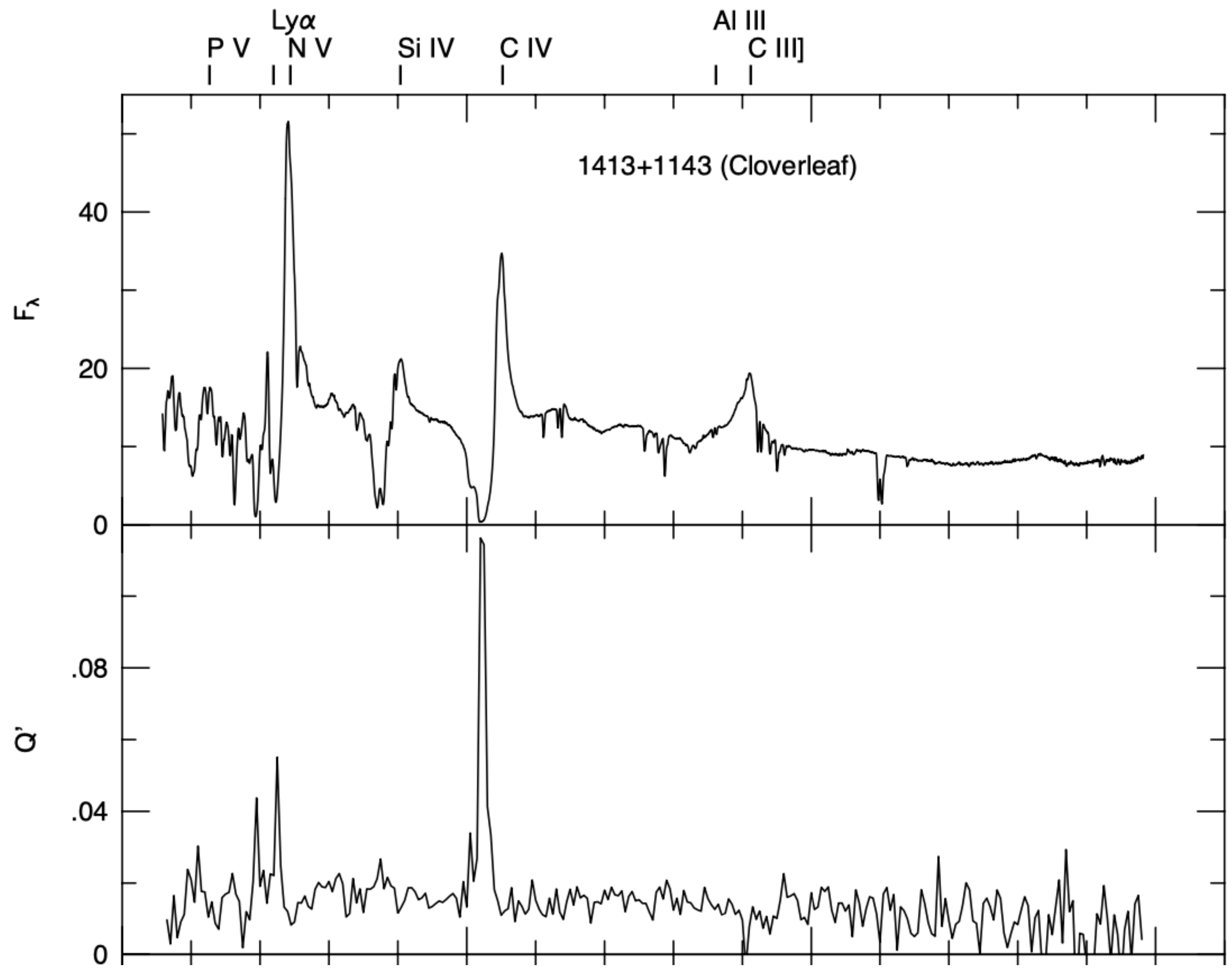

Ogle+ 1999

Feedback from BAL Outflows?

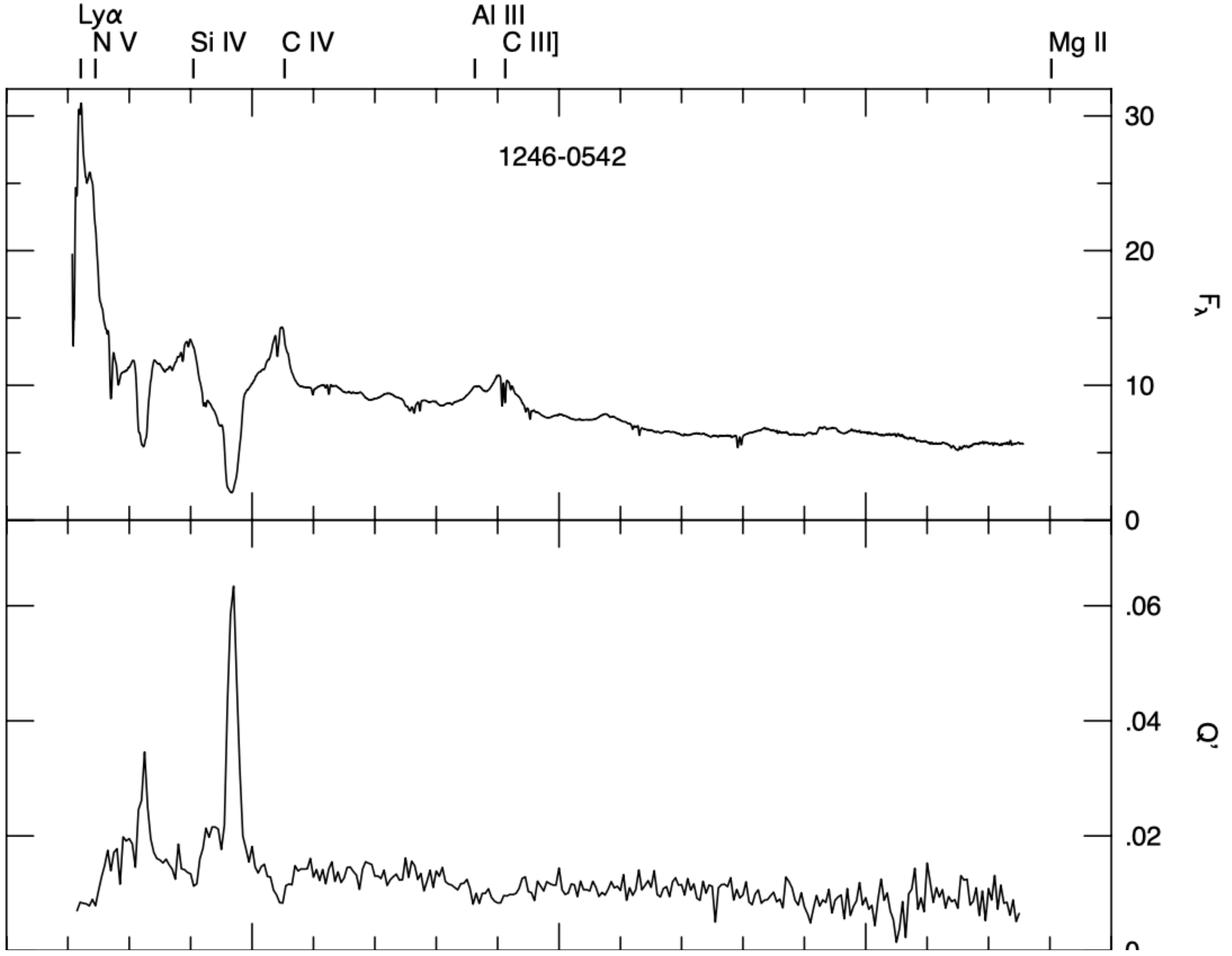

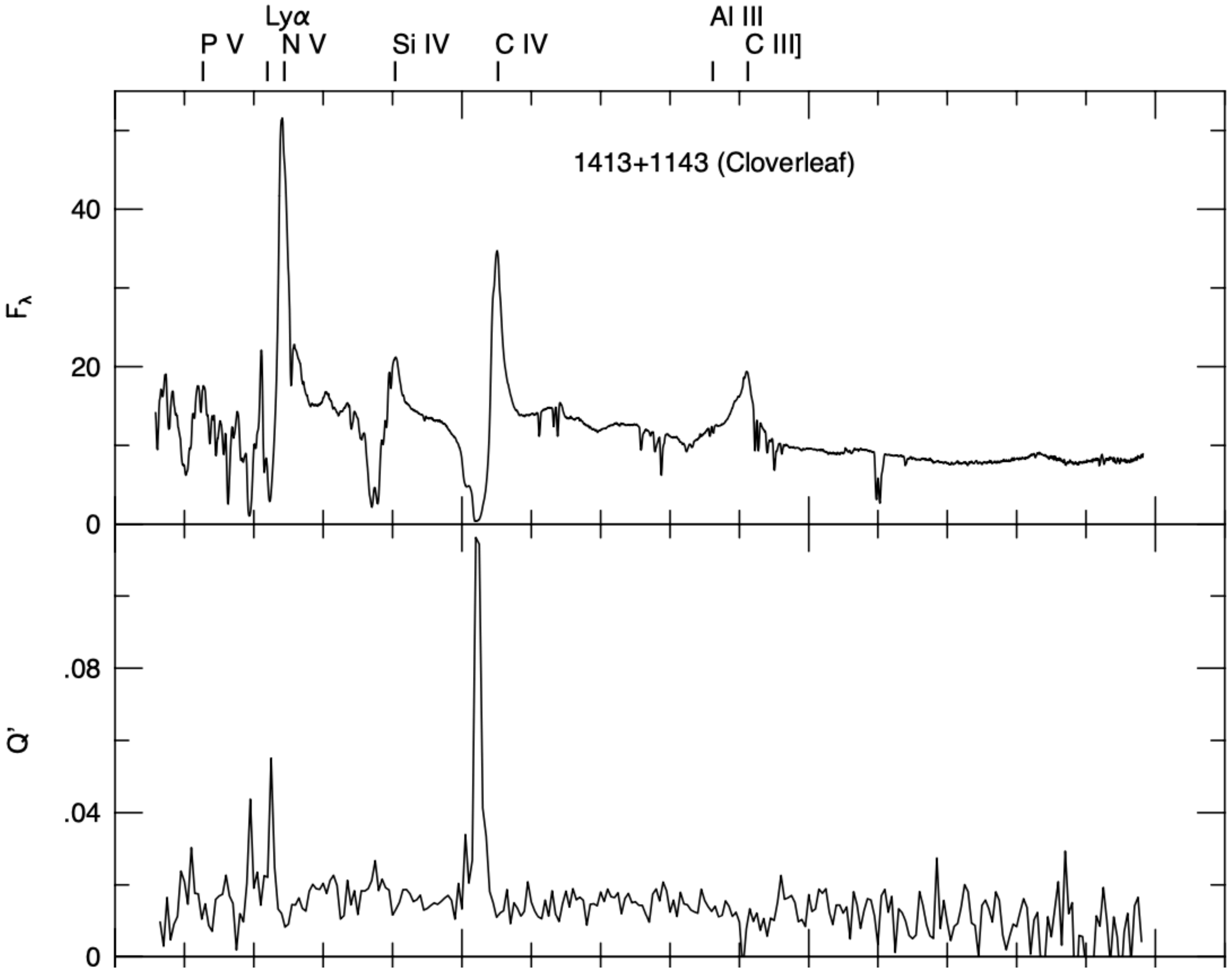

Feedback from BAL Outflows?

- Wind luminosity = 1/2 dM/dt v^2 = 1/2 $\Omega R^2 \rho v^2$
- Momentum loss rate = dM/dt v = $\Omega R^2 \rho v$
- Measure v directly
- Estimate ρ
- Need R
- R~10^{17}cm, D~200Mpc, 10 microarcseconds
- V~13.8

Binary SMBHs

- In future years, we expect to detect some binary SMBH's as individual sources with PTAs.
- Already some candidate binaries exist:

PG 1302-102

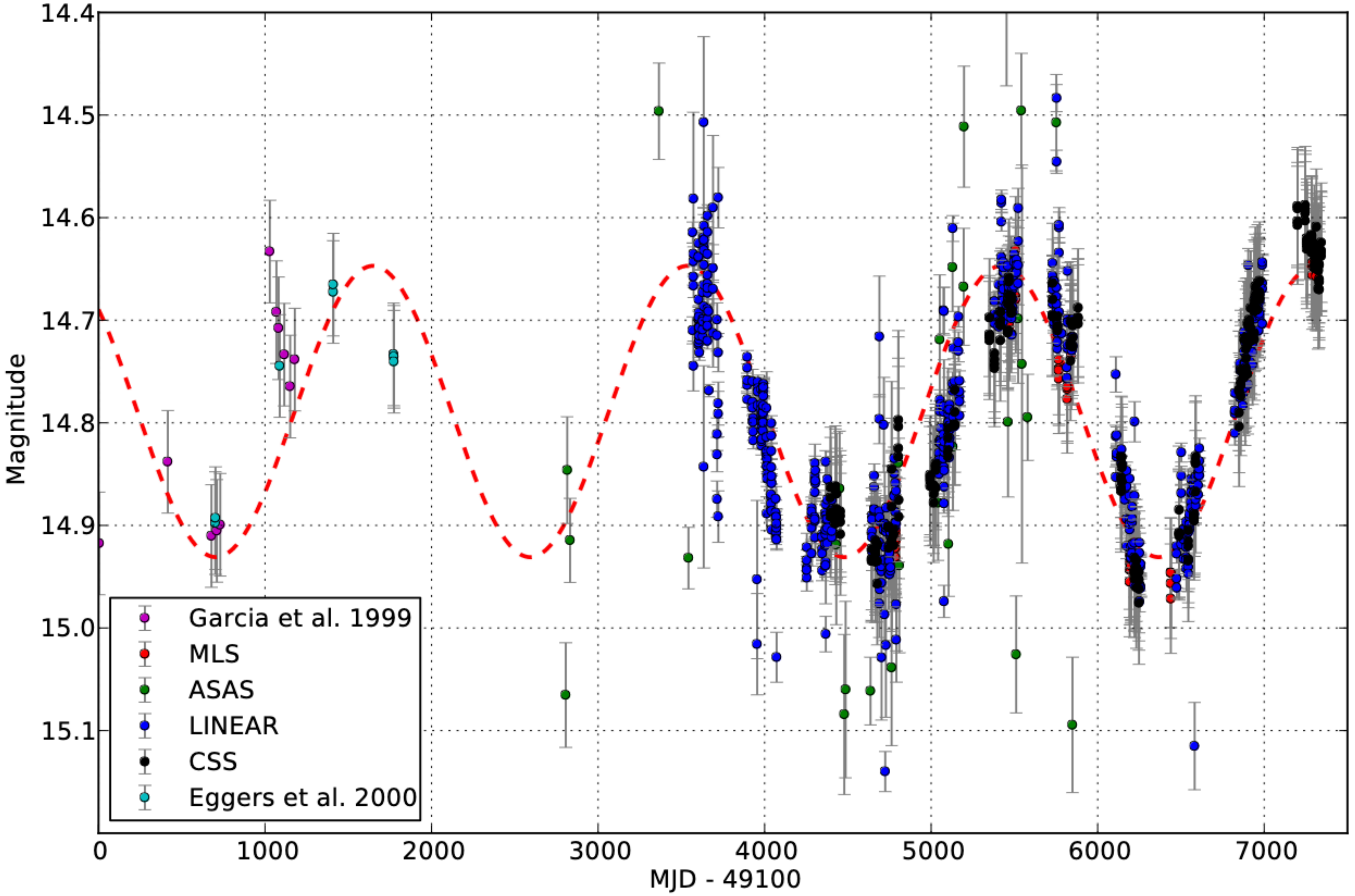

Graham et al. (2015)

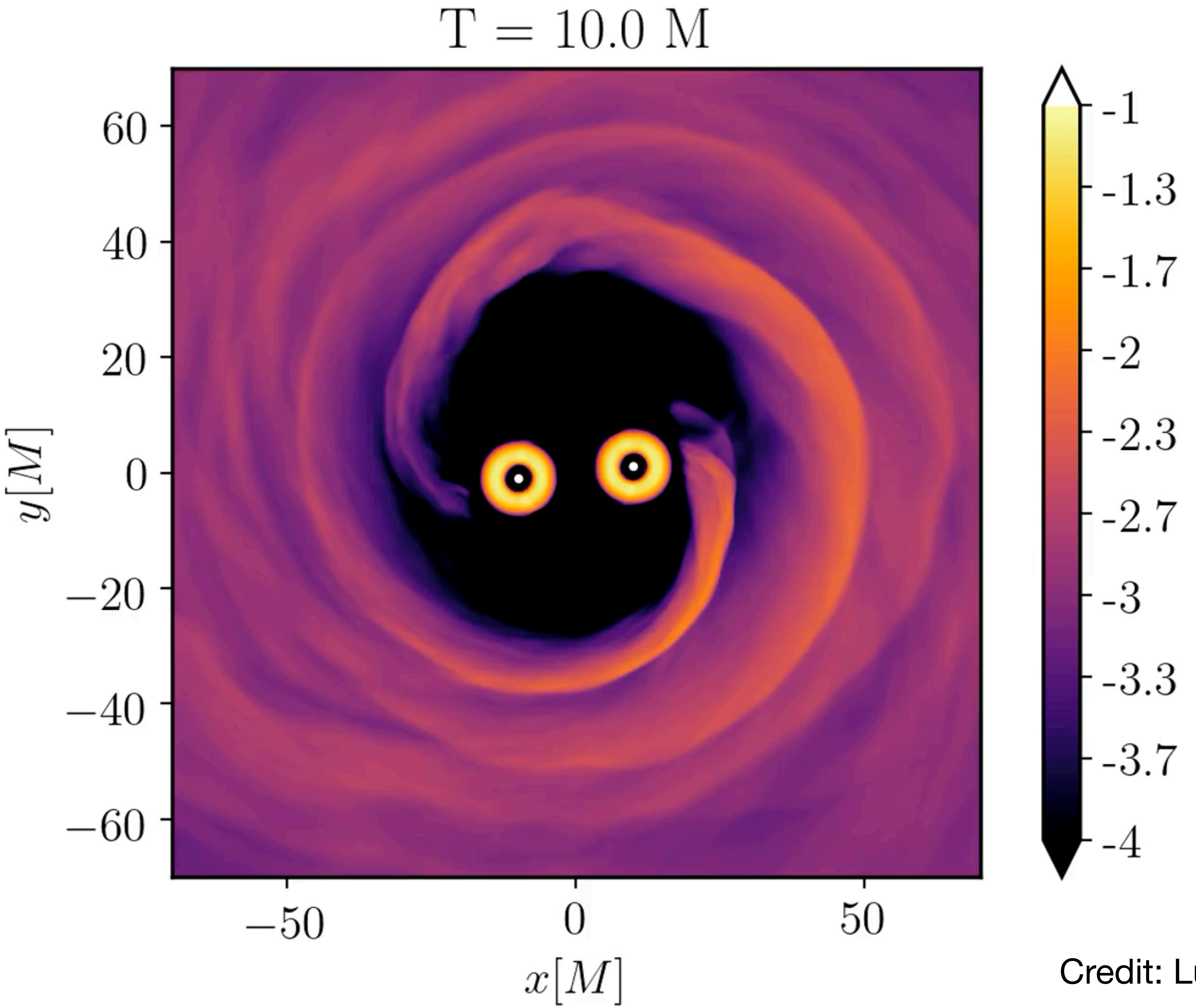

Credit: Luciano Combi

Binary SMBHs

Two supermassive Black Holes: OJ 287

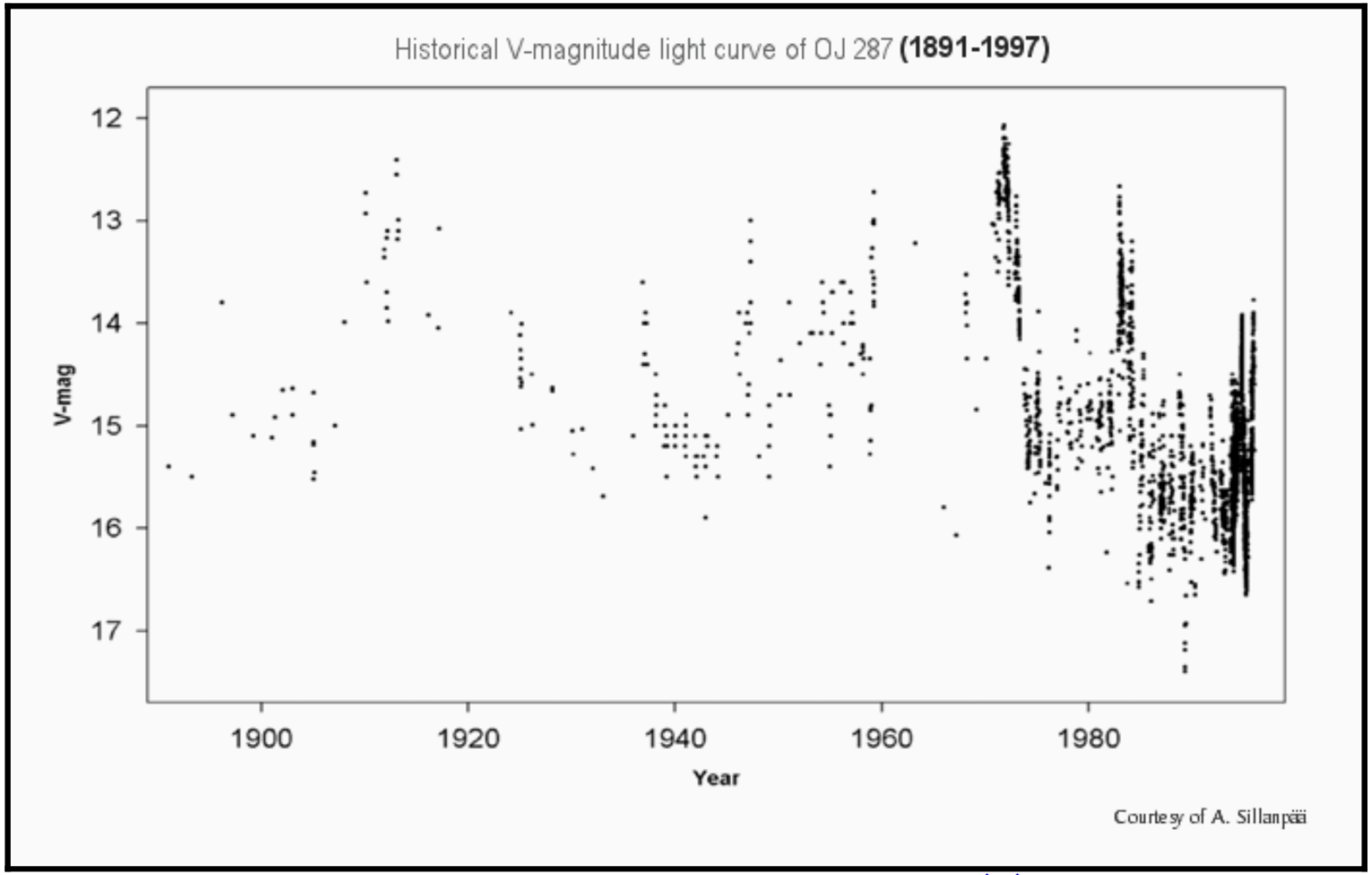

Light Curve 1891-1997 - courtesy [A. Sillanp��]

Binary AGN

Two supermassive Black Holes: OJ 287

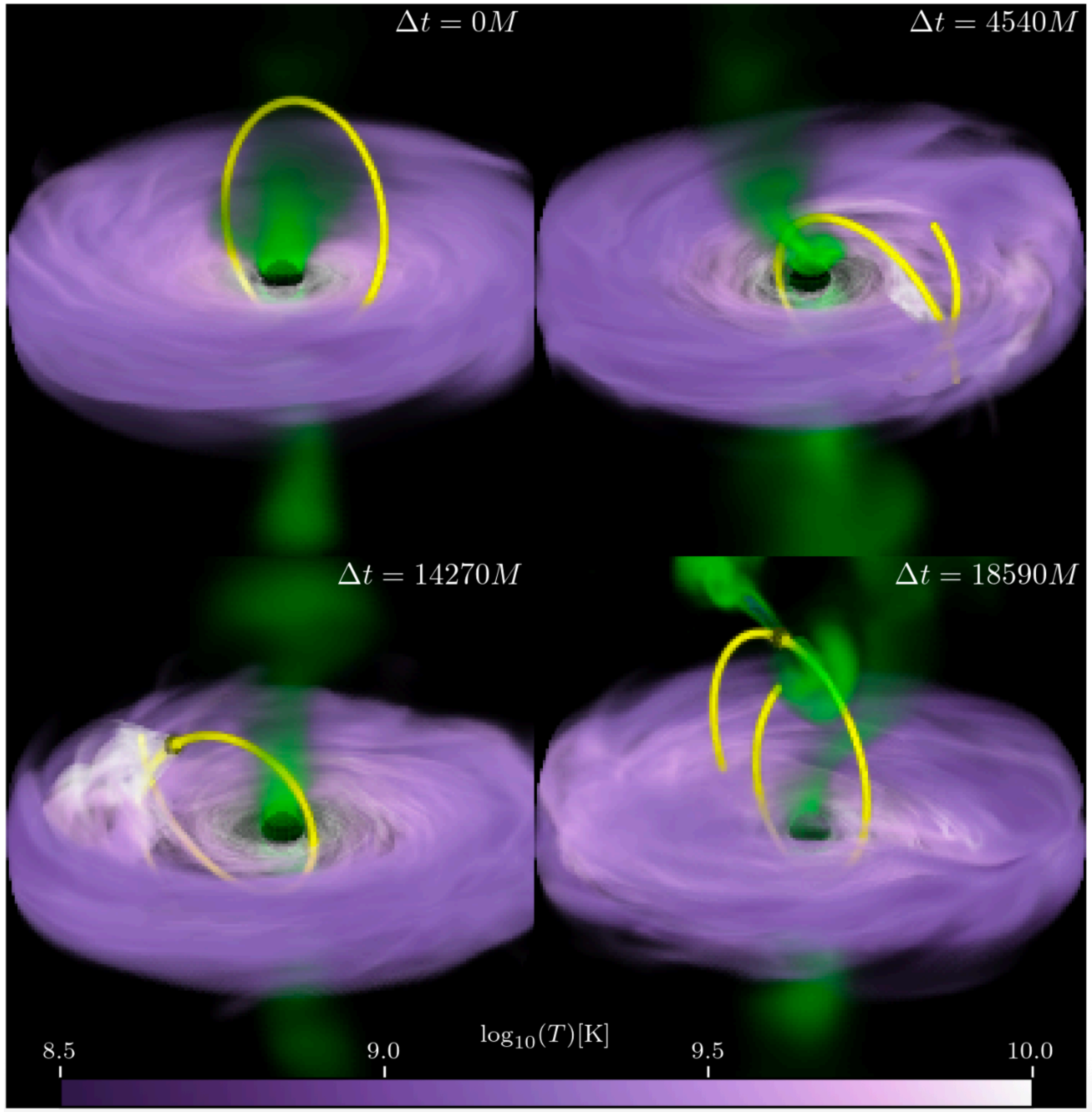

Ressler et al. (2025)

Binary AGN

Two supermassive Black Holes: OJ 287

Ressler et al. (2025)

Binary AGN

NGC 5548

V=13.7

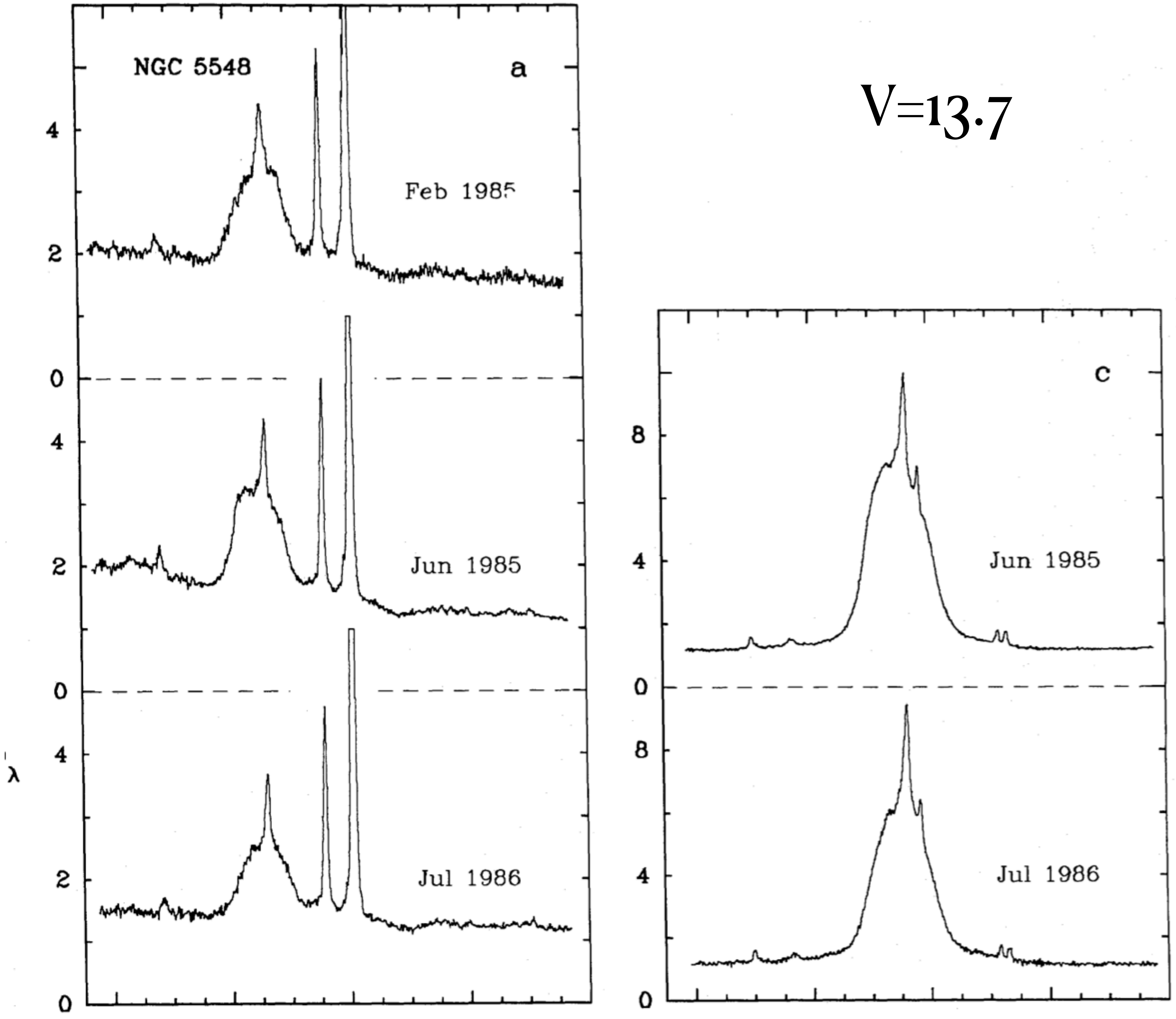

Green Peas

Lin et al. (2025) ApJ 980 L34

V=20

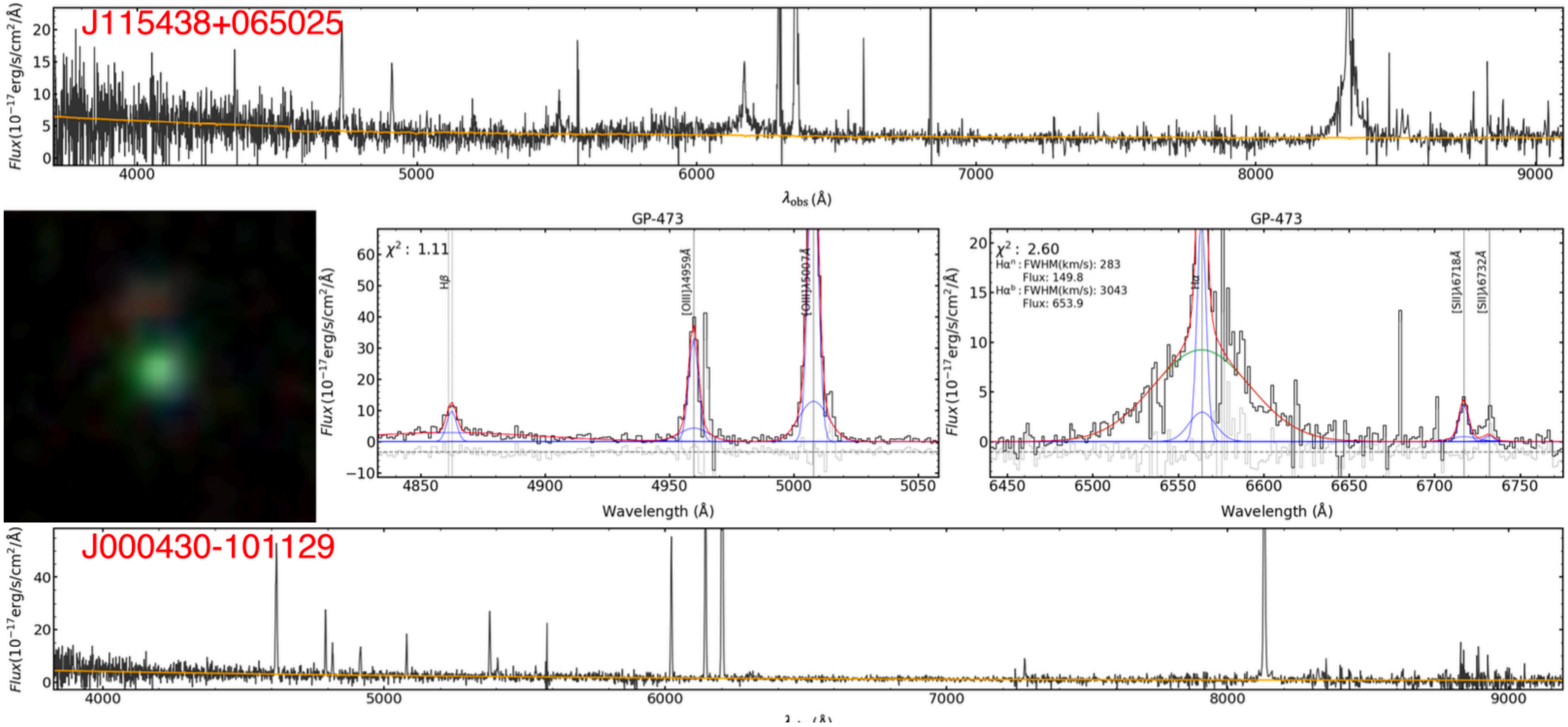

Little Red Dots (LRDs)

Liu et al. 2025

V>25

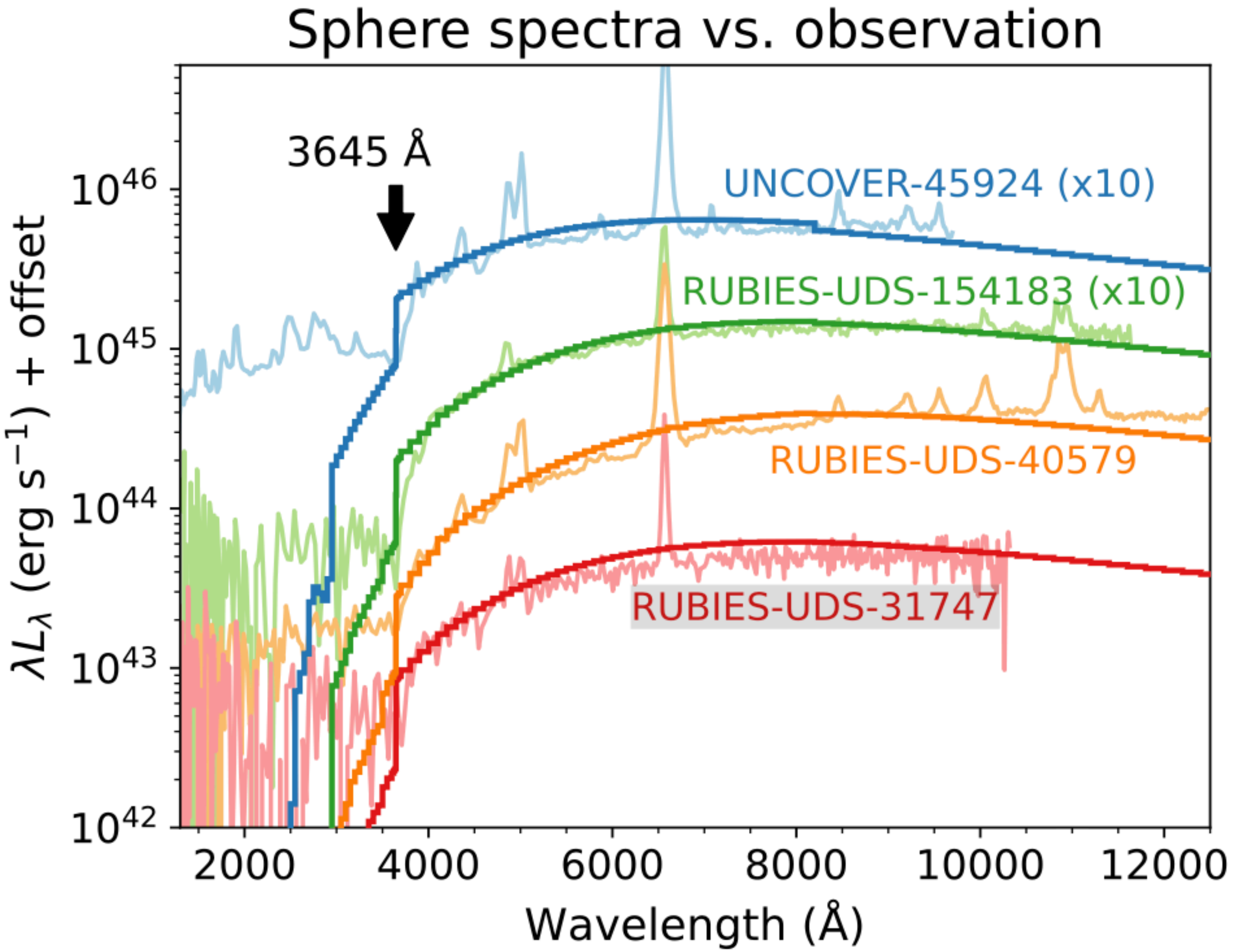

Asteroseismology

Internal differential rotation

- Solar dynamo is driven by differential rotation
- Stellar magnetic fields produce x-rays and the bulk of the UV flux
- X-rays and UV evaporate protostellar disks
- X-rays and UV can strip planetary atmospheres

Larson & Schou (2018)

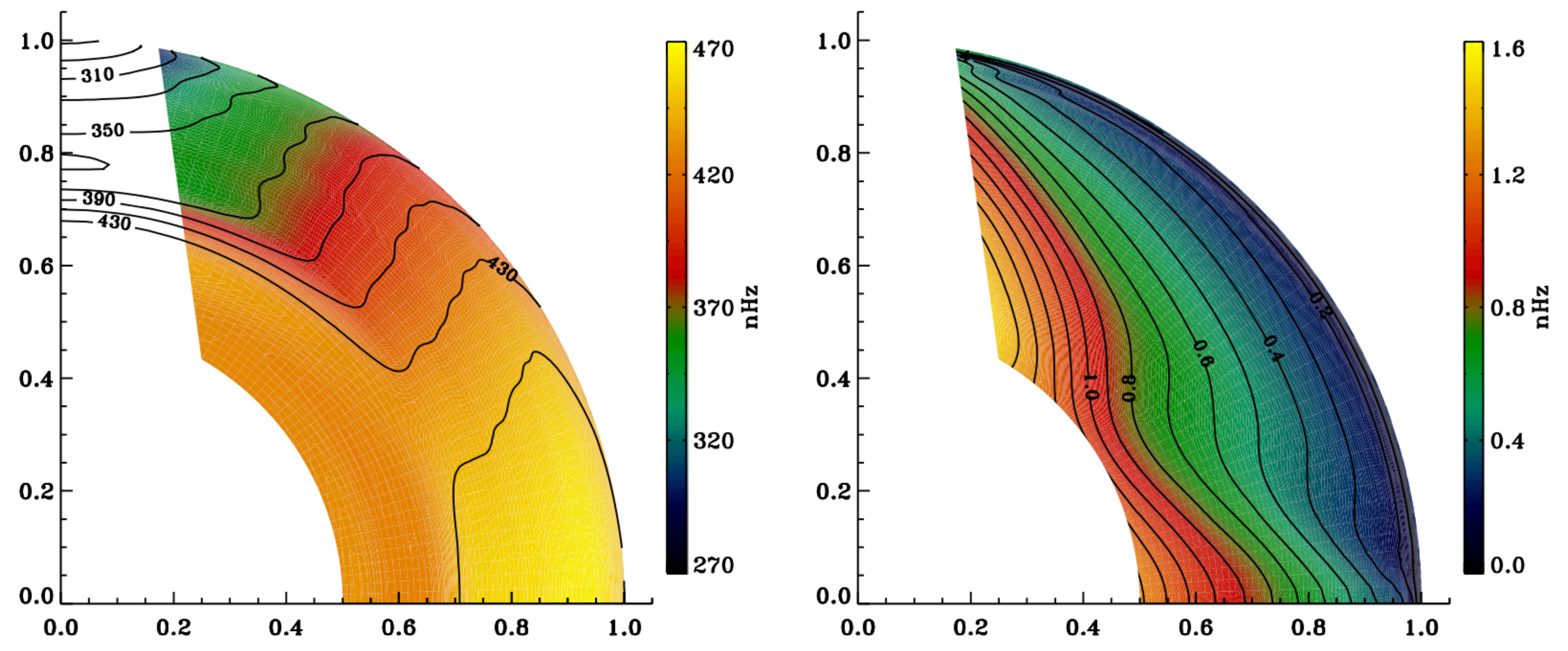

Figure 29 Internal rotation (*left*) and the corresponding errors (*right*) derived from the MDI full-disk analysis averaged over all Dynamics Runs. We have erased color from the regions where estimates of rotation are deemed unreliable; contours are retained on the left for ease of labeling.

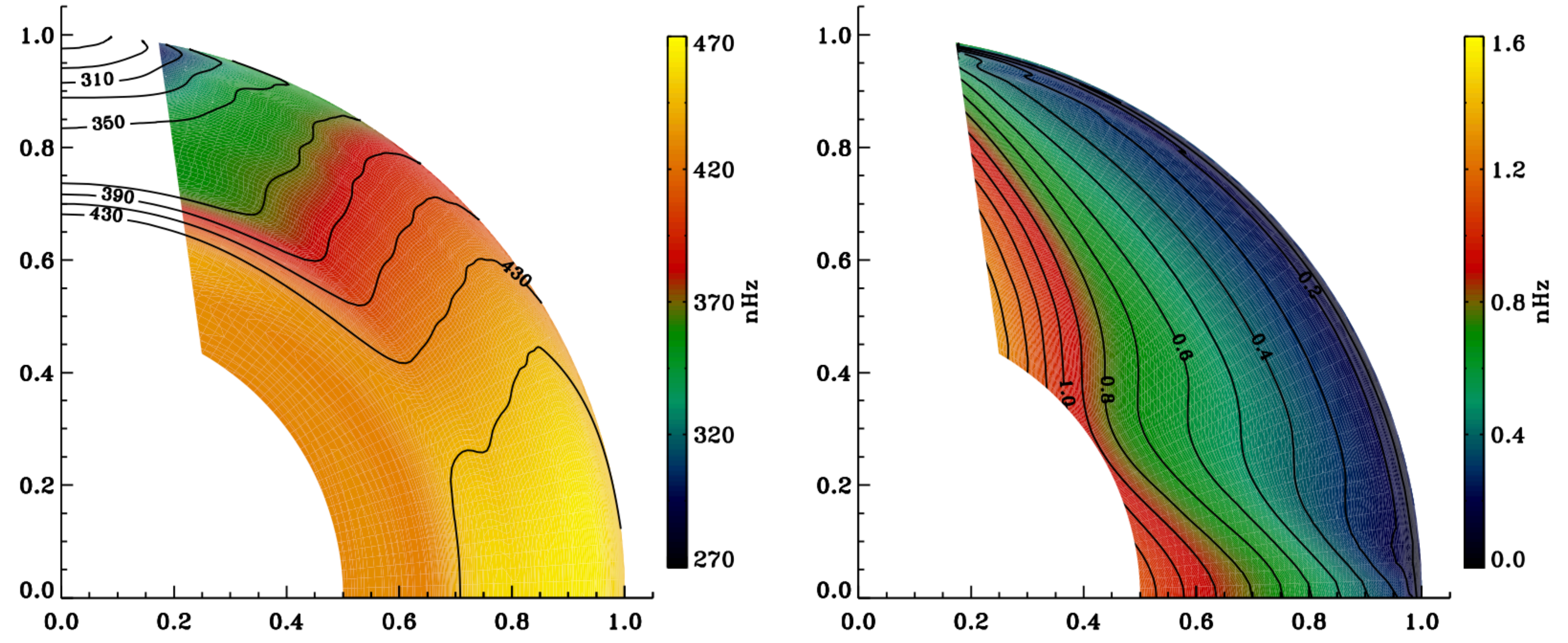

Figure 30 Internal rotation (*left*) and the corresponding errors (*right*) derived from an average over the first six years of the HMI 72-day analysis. We have erased color from the regions where estimates of rotation are deemed unreliable; contours are retained on the left for ease of labeling.

Helioseismology

Internal differential rotation

230 M. LAZREK ET AL.

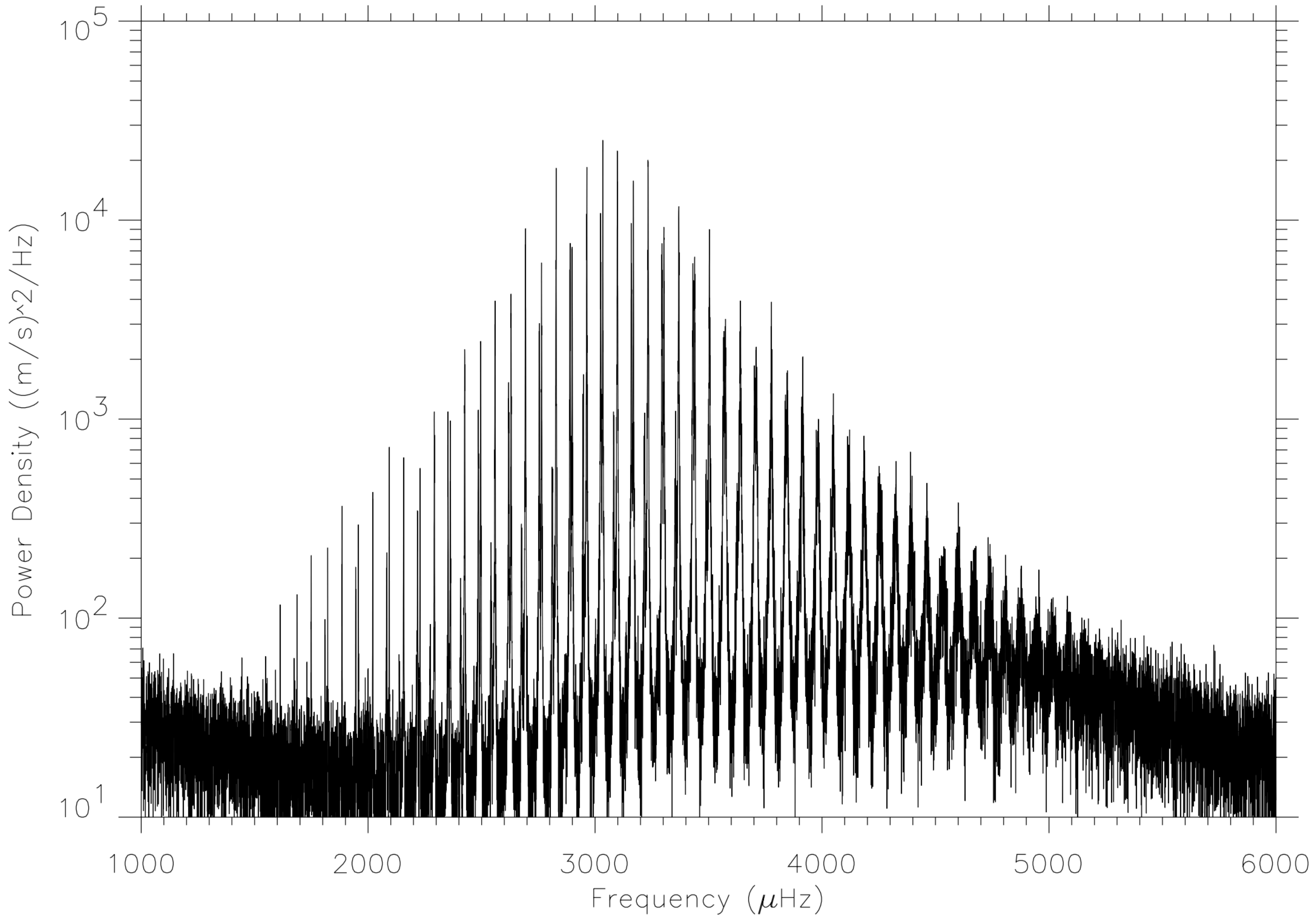

Figure 1. The acoustic *p*-mode spectrum of the Sun, as measured using the first eight months of GOLF data. At 3 mHz the ratio S/N is ∼3000.

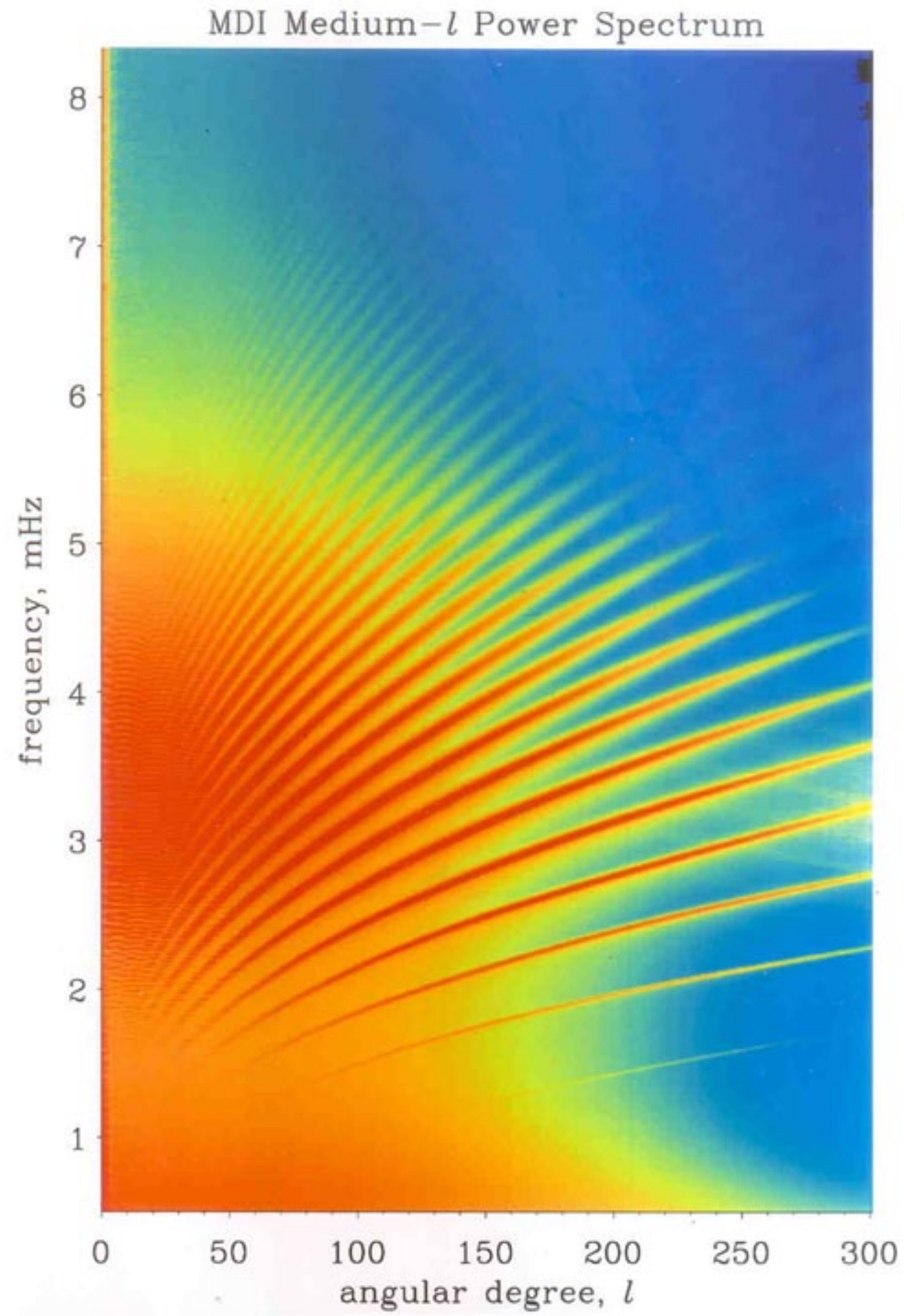

- Resolved stellar oscillation velocity power spectra

Helioseismology

Internal differential rotation

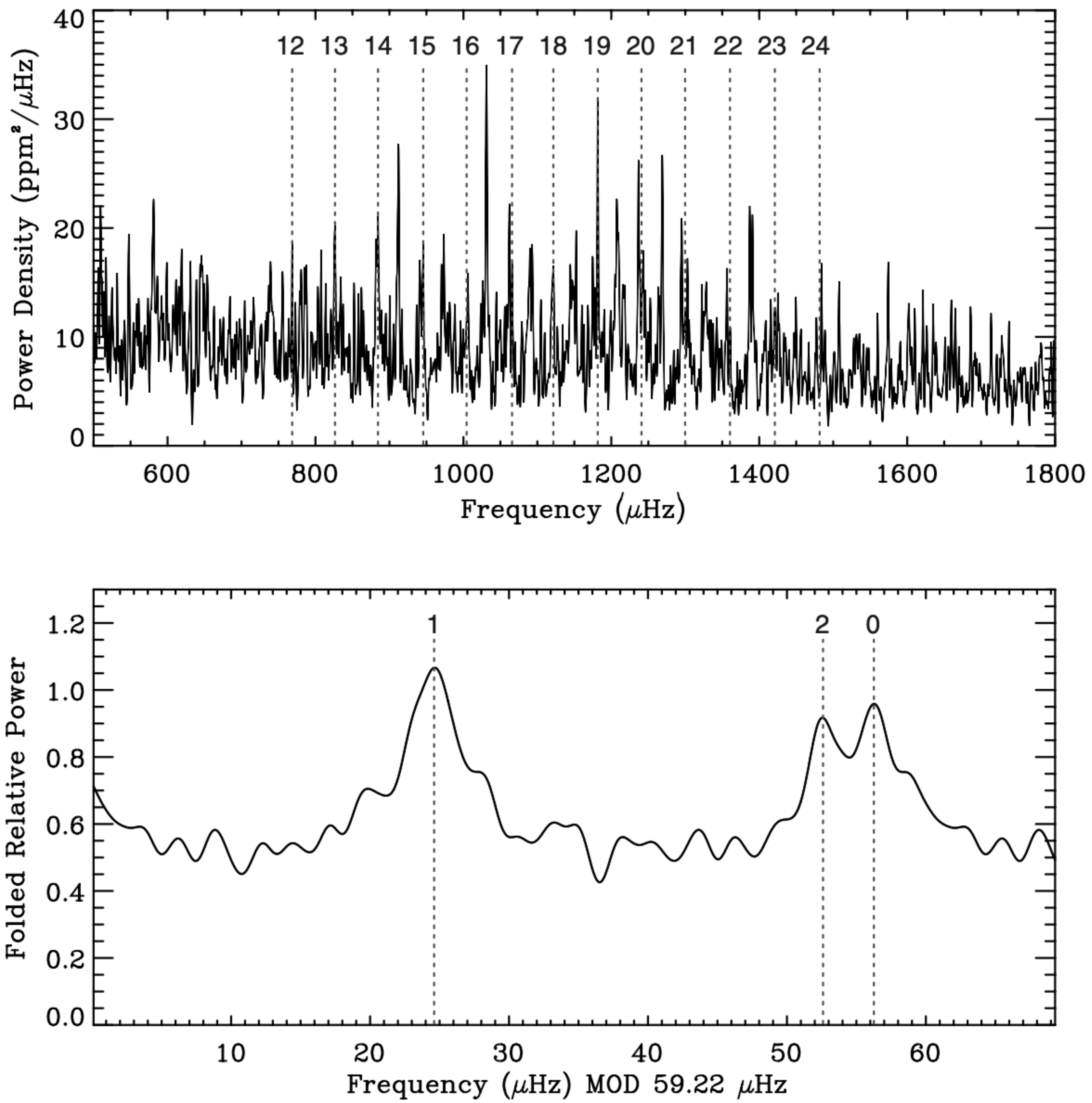

Helioseismology

Internal differential rotation

SOLAR p-MODE FREQUENCY SPLITTINGS 1093

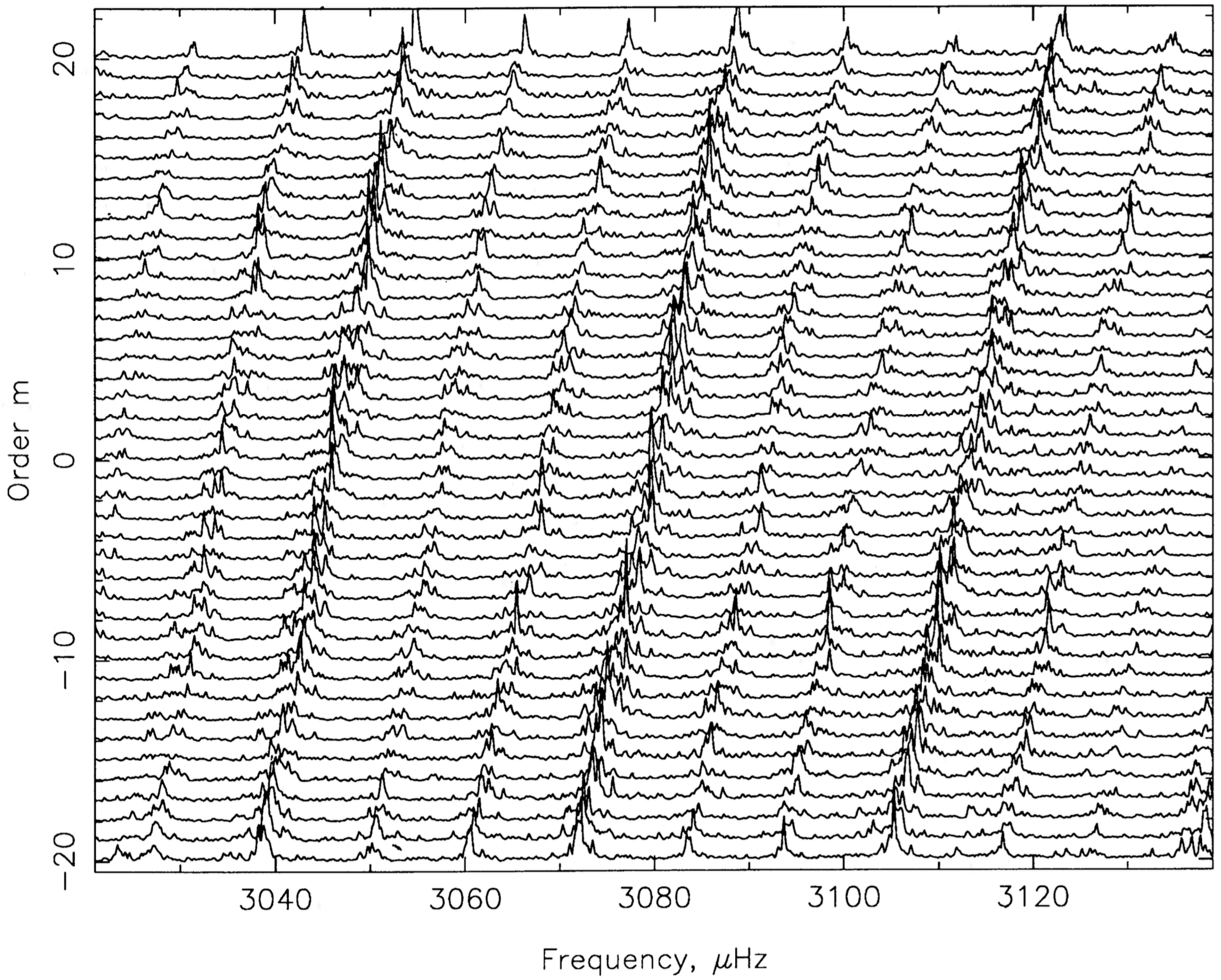

Libbrecht 1989

Helioseismology

Internal differential rotation

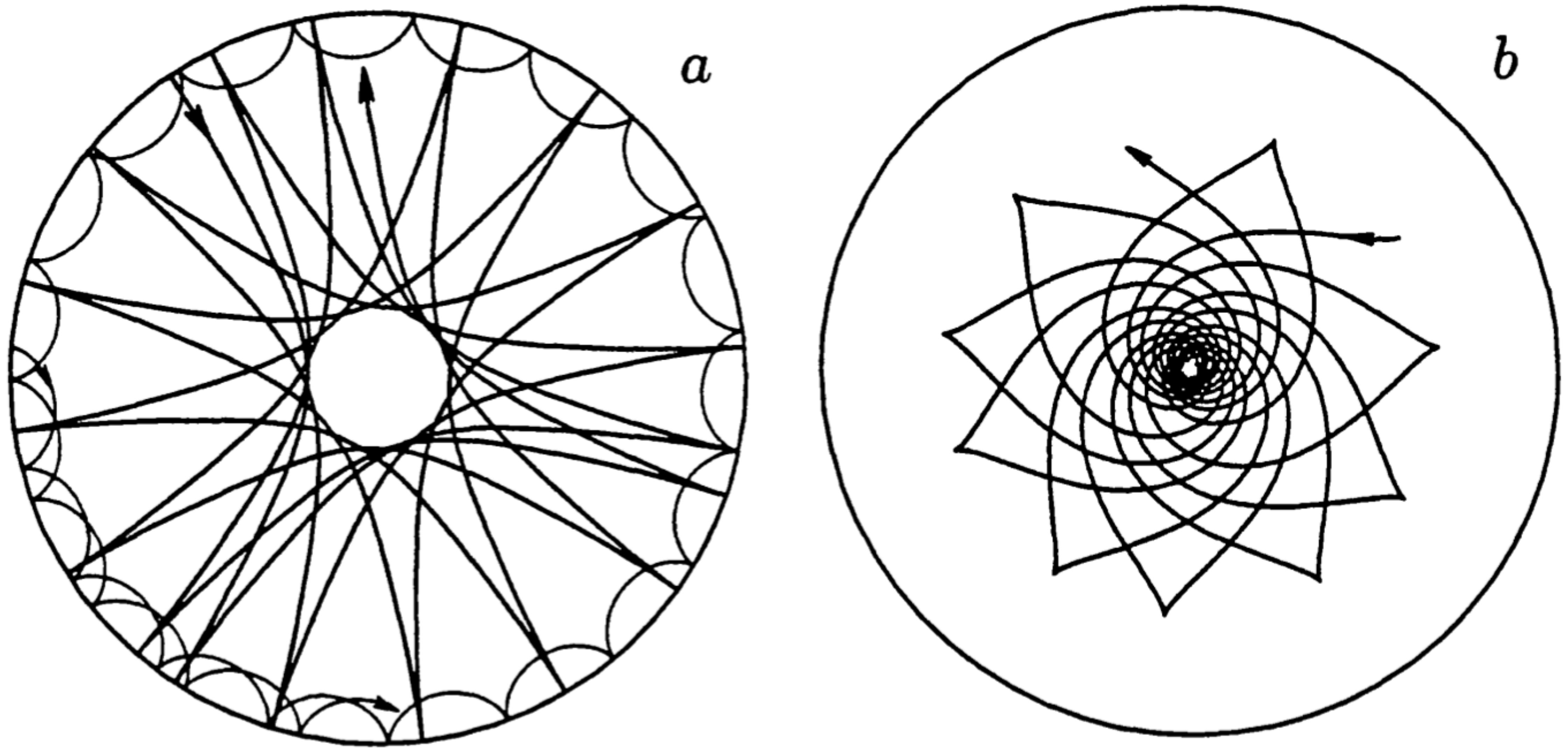

Figure 2 Ray paths in the standard model of the sun represented by the continuous line in Figure 1: (*a*) for two acoustic waves; the more deeply penetrating wave is p_8 ($l = 2$) and the shallower wave is p_8 ($l = 100$); (*b*) for the gravity wave g_{10} ($l = 5$). Note that the number of reflections per revolution is not integral, and indeed is almost never rational, so the ray paths

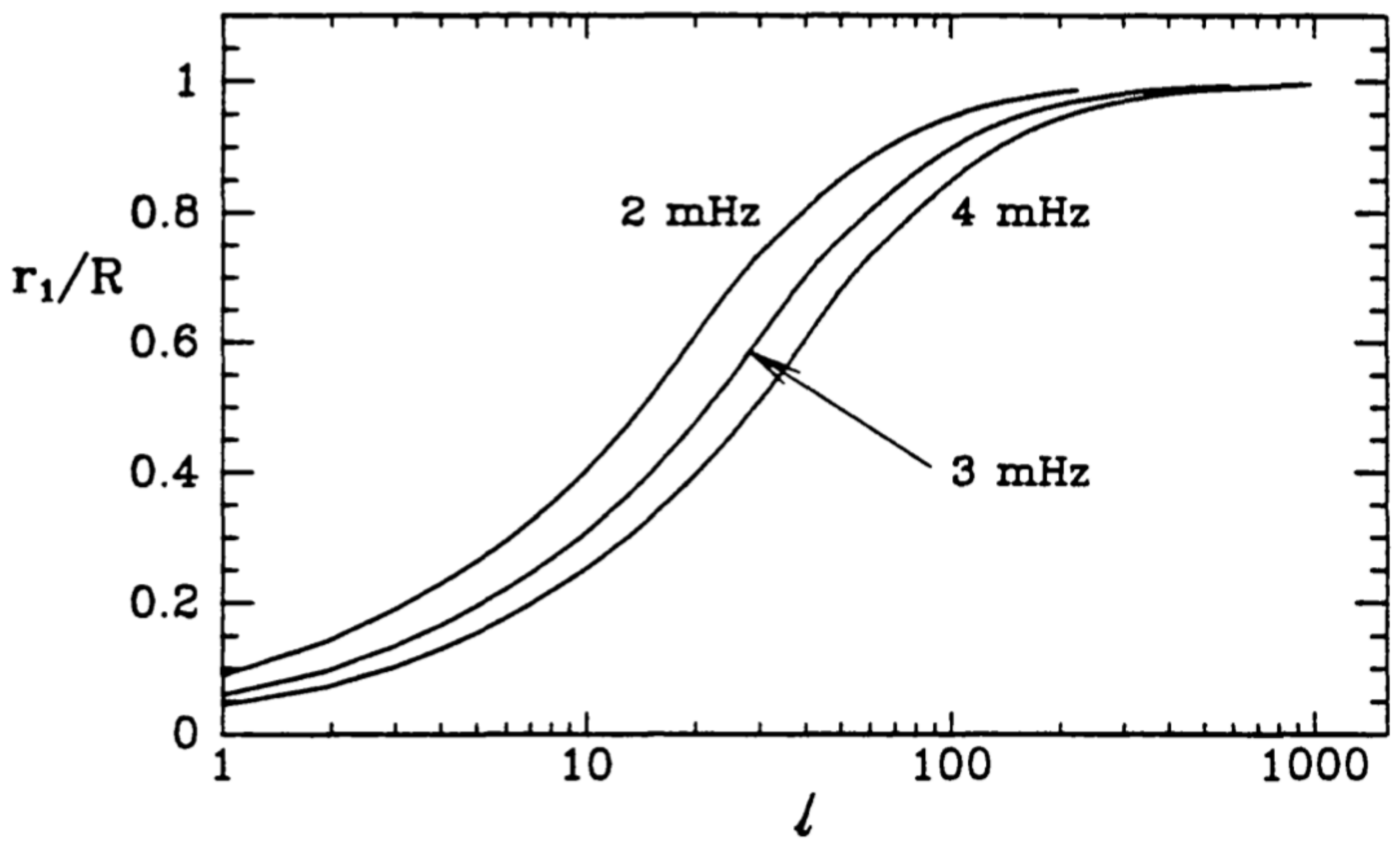

Figure 3 Lower turning points for p modes of a solar model, determined by the vanishing of κ, plotted against degree l for the three cyclic frequencies $\nu = \omega/2\pi = 2, 3, 4$ mHz. The curves for 2 and 3 mHz terminate at the lowest-order modes, at values of l determined by Equation 3.2 with $n = 1$.

Helioseismology

Sound speed v. R

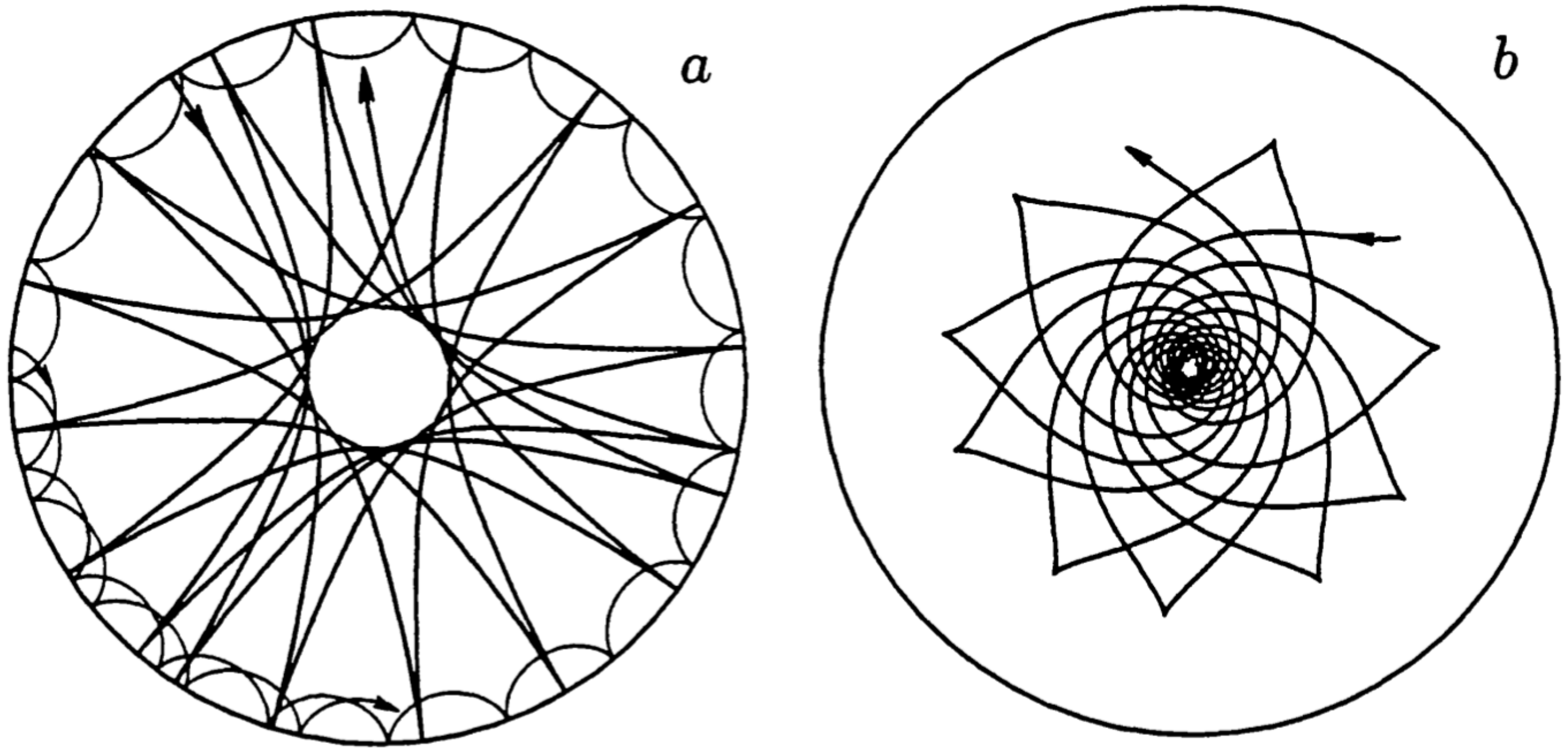

Figure 2 Ray paths in the standard model of the sun represented by the continuous line in Figure 1: (*a*) for two acoustic waves; the more deeply penetrating wave is p_8 ($l = 2$) and the shallower wave is p_8 ($l = 100$); (*b*) for the gravity wave g_{10} ($l = 5$). Note that the number of reflections per revolution is not integral, and indeed is almost never rational, so the ray paths

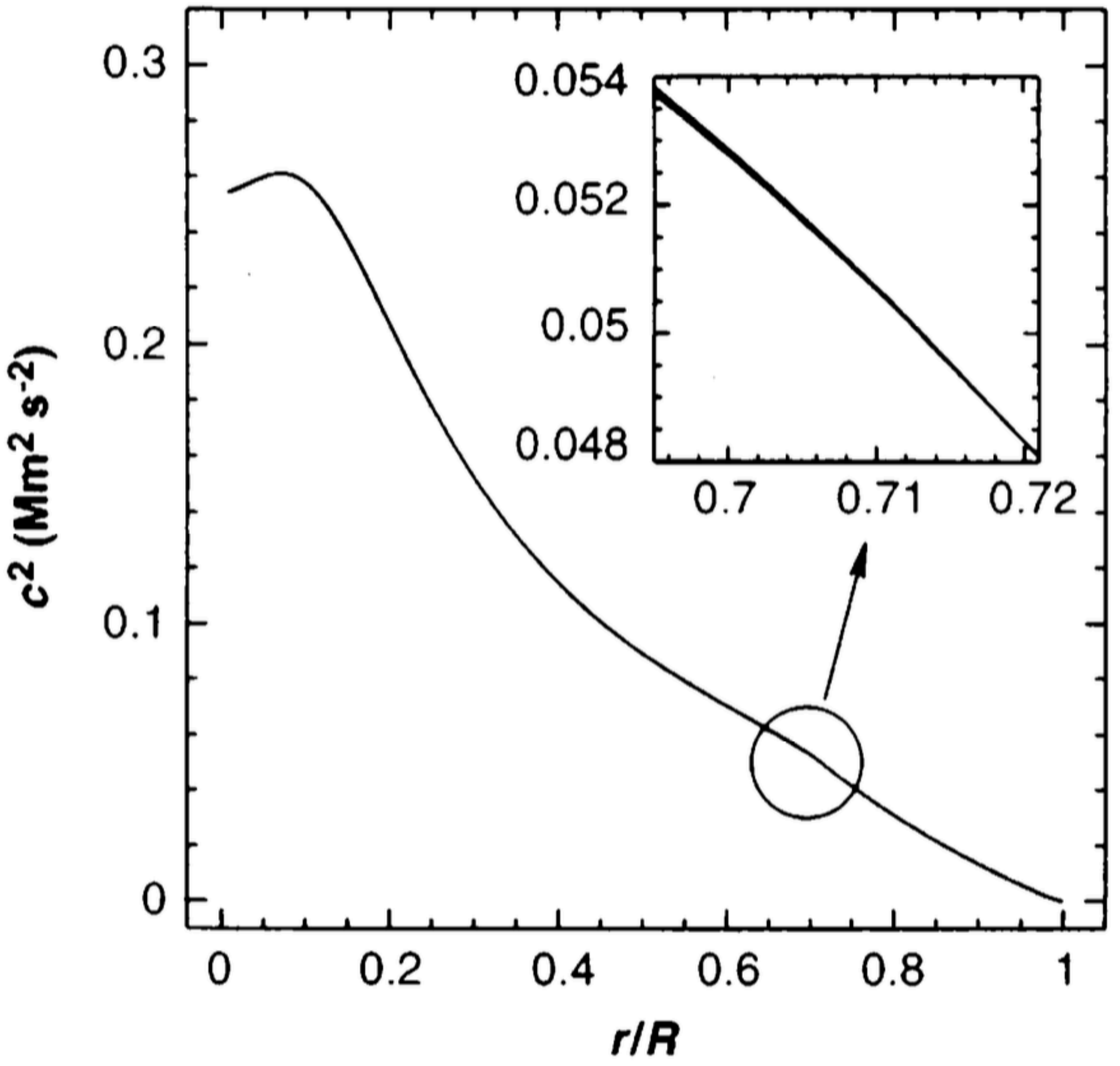

Fig. 3. The dashed curve is the square of the spherically averaged sound speed in the sun. The solid curve corresponds to a standard theoretical model. The magnitudes of the slopes of the curves are lower immediately beneath the convection zone, where the temperature gradient is too small to drive the instability. The inset shows that the convectively unstable region of relatively high slope extends somewhat more deeply into the sun than it does in the model.